Geophysical Journal International

Geophys. J. Int. (2015) **200,** 227–243
GJI Geodynamics and tectonics

doi: 10.1093/gji/ggu392

The anticorrelated velocities of Africa and India in the Late Cretaceous and early Cenozoic

Steven C. Cande[1] and Philippe Patriat[2]

[1]*Scripps Institution of Oceanography, La Jolla, CA* 92093-0220*, USA. E-mail: scande@ucsd.edu*
[2]*Laboratoire de Geosciences Marines, Institut de Physique du Globe de Paris,* 4 *place Jussieu, F*-75252 *Paris cedex* 05*, France*

Accepted 2014 October 7. Received 2014 October 3; in original form 2014 May 26

Downloaded from https://academic.oup.com/gji/article/200/1/227/749250 by guest on 18 February 2022

SUMMARY

We present a revised interpretation of magnetic anomalies and fracture zones on the Southwest Indian Ridge (SWIR; Africa–Antarctica) and the Southeast Indian Ridge (SEIR; Capricorn–Antarctica) and use them to calculate 2-plate finite rotations for anomalies 34 to 20 (84 to 43 Ma). Central Indian Ridge (CIR; Capricorn–Africa) rotations are calculated by summing the SWIR and SEIR rotations. These rotations provide a high-resolution record of changes in the motion of India and Africa at the time of the onset of the Reunion plume head. An analysis of the relative velocities of India, Africa and Antarctica leads to a refinement of previous observations that the speedup of India relative to the mantle was accompanied by a slowdown of Africa. The most rapid slowdown of Africa occurs around Chron 32Ay (71 Ma), the time when India's motion relative to Africa notably starts to accelerate. Using the most recent Geomagnetic Polarity Timescale (GTS12) we show that India's velocity relative to Africa was characterized by an acceleration from roughly 60 to 180 mm yr^{-1} between 71 and 66 Ma, a short pulse of superfast motion (∼180 mm yr^{-1}) between 66 and 63 Ma, an abrupt slowdown to 120 mm yr^{-1} between 63 and 62 Ma, and then a long period (63 to 47 Ma) of gradual slowing, but still fast motion (∼100 mm yr^{-1}), which ends with a rapid slowdown after Chron 21o (47 Ma). Changes in the velocities of Africa and India with respect to the mantle follow a similar pattern. The fastest motion of India relative to the mantle, ∼220 mm yr^{-1}, occurs during Chron 29R. The SWIR rotations constrain three significant changes in the migration path of the Africa–Antarctic stage poles: following Chron 33y (73 Ma), following Chron 31y (68 Ma), and following Chron 24o (54 Ma). The change in the migration path of the SWIR stage poles following Chron 33y is coincident with the most rapid slowdown in Africa's motion. The change in the migration path after Chron 31y, although coincident with the most rapid acceleration of India's northward motion, may be related to changes in ridge push forces on the SWIR associated with the onset of extension along the Bain transform fault zone. The initial slowdown in India's motion relative to Africa between 63 and 62 Ma is more abrupt than predictions based on published plume head force models, suggesting it might have been caused by a change in plate boundary forces. The abrupt change in the migration path of the SWIR stage poles after Chron 24o is not associated with major changes in the velocities of either Africa or India and may reflect Atlantic basin plate motion changes associated with the arrival at the Earth's surface of the Iceland plume head. The abruptness of India's slowdown after Chron 21o is consistent with a collision event.

Key words: Plate motions; Kinematics of crustal and mantle deformation; Indian Ocean.

1 INTRODUCTION

Indo-Atlantic Plate kinematics during the Late Cretaceous and early Cenozoic were characterized by two events: a period of unusually rapid motion of India starting around 68 Ma and lasting until roughly 50 Ma, and an unusual slowdown of Africa starting around 70 Ma (Cande & Stegman 2011). The synchroneity of India's fastest motion (66 to 63 Ma) with the maximum outpouring of Deccan flood basalts (Pande 2002; Chenet *et al.* 2007) has been noted by many (Richards *et al.* 1989; Duncan & Richards (1991), leading to the suggestion that the speedup was caused by the arrival of the Reunion plume head at the Earth's surface (van Hinsbergen *et al.* 2011). The

© The Authors 2014. Published by Oxford University Press on behalf of The Royal Astronomical Society.

slowdown of Africa starting at 70 Ma has not received as much attention, but the near synchroneity of this event with India's speedup is striking and suggests that it too may have been driven by the Reunion plume head (Cande & Stegman 2011). Establishing the connection, if any, between India and Africa's motions remains an outstanding problem.

Understanding the possible connections between changes in the motion of India and Africa and the arrival of the Reunion plume head requires an accurate portrayal of plate motions on the Southwest Indian Ridge (SWIR), Southeast Indian Ridge (SEIR) and Central Indian Ridge (CIR). The fracture zones and magnetic anomalies on the SWIR contain a detailed record of the complex plate motions between Africa and Antarctica while the marine geophysical constraints from the CIR and SEIR represent the most accurate recording of the speedup and slowdown of India. Although the SWIR constraints have been studied extensively (e.g. Molnar *et al.* 1988; Royer *et al.* 1988; Nankivell 1997; Bernard *et al.* 2005; Cande *et al.* 2010), these studies do not provide the detail needed to look at changes in plate motion at critical times. In particular the rotations do not define the Africa–Antarctica Plate motion changes in detail at the time of the onset of the Reunion plume head around 68 Ma, nor do they accurately define the dramatic changes in the fracture zones on the SWIR around Chron 24o (54 Ma; Ogg 2012).

In this paper, we re-examine the marine geophysical and satellite gravity constraints on spreading on the SWIR and SEIR and calculate closely spaced finite rotations between Chrons 34y (84 Ma) and 20o (43 Ma). We show that the revised SWIR stage poles define significant changes in SWIR motion after Chrons 33y (73 Ma), 31y (68 Ma) and 24o (54 Ma). We then use the rotations to look in detail at the relative motion of India, Africa and Antarctica between 84 and 43 Ma. We show that recent changes to the geomagnetic polarity timescale (GPTS) as detailed in Ogg 2012 (GTS12) lead to significant changes in the perceived character of the motion of India.

2 BACKGROUND

The SWIR contains a detailed record of the motion of the African Plate relative to Antarctica since the late Jurassic (Bergh 1971). Although the early interpretations of the spreading history between Africa and Antarctica modelled the Cenozoic era with a single Euler pole (e.g. Norton & Sclater 1979), Patriat *et al.* (1985) recognized that there was a major change in the relative motion of Africa and Antarctica in the Late Cretaceous and again in the early Cenozoic. These changes were characterized by a gradual counter-clockwise change in spreading direction starting around Chron 32 (72 Ma) followed by a more sudden clockwise change in direction around Chron 24 (54 Ma). This time also corresponded to a period of slower spreading rates. These changes in spreading rate and direction had a dramatic effect on all of the SWIR transform faults and particularly on the large offset Bain transform fault. The Late Cretaceous counter-clockwise change in direction put the Bain transform fault into extension and led to the development of a large number of small offset ridge segments and fracture zone splays (Royer *et al.* 1988). These small offset ridge segments disappeared after the clockwise change in spreading direction around Chron 24 (54 Ma) which restored the original spreading direction. Several more recent studies (Molnar *et al.* 1988; Nankivell 1997; Bernard *et al.* 2005; Cande *et al.* 2010) have re-examined plate motions on the SWIR, but none of them provide an adequately detailed set of rotations between Chrons 34y and 20 to accurately define the spreading rate variations and changes in azimuth of the SWIR fracture zones that reflect the prolonged slowdown and speedup of Africa.

A potential problem in using data from the SWIR is the presence of one or more late Cenozoic diffuse plate boundaries near the ridge axis within the African Plate. Several studies have proposed that fitting Euler rotations to magnetic anomalies along the SWIR requires that Africa be considered as two rigid plates, the Nubia Plate in the west and the Somalia Plate to the east (Chu & Gordon 1999; Lemaux *et al.* 2002; Royer *et al.* 2006), with a plate boundary that intercepts the SWIR near the Bain transform. More recently Horner-Johnson *et al.* (2007) showed that recent spreading rates along the SWIR ridge axis are best fit by three plates, inserting the Lwandle Plate between the Nubia and Somalia plates. However, Patriat *et al.* (2008) and Cande *et al.* (2010) showed that the effect of the Lwandle–Nubia and Nubia–Somalia rotations are relatively small on anomalies 6 and older; we do not use them in the analysis presented here. Because we do not distinguish between the Somalia, Lwandle and Nubia Plate in this paper, we will refer to all three plates as the African Plate.

Spreading between Antarctica and India (Australia) currently occurs along the SEIR from the Indian Ocean Triple Junction (IOTJ) east to the Macquarie triple junction. However prior to the change in India Plate motion at roughly Chron 20 (43 Ma), India and Australia were two plates separated by a spreading ridge that passed through the Wharton Basin and north of Australia (McKenzie & Sclater 1971; Liu *et al.* 1983). The early Cenozoic spreading between India, Africa and Antarctica on the CIR and SEIR was mapped in detail by Patriat (1987) and Patriat & Segoufin (1988). A set of rotations going back to anomaly 34y using constraints from satellite altimetry data was calculated by Royer & Sandwell (1989). Additional constraints on CIR and SEIR spreading in the early Cenozoic, focusing on the location of the L'Astrolabe and La Boussole fracture zones and the trace of the IOTJ on the Indian Plate, were given in Dyment (1993). A survey of the African flank of the CIR southeast of Reunion mapped the change in spreading direction around Chron 20 as recorded in the topography and magnetic field (Dyment 1998). Cande *et al.* (2010) calculated rotations for anomalies 18o to 29o as part of their 3-plate analysis of the IOTJ.

A difficulty in calculating rotations for the SEIR is that there has been considerable deformation within the Indian Plate over the last 20 Ma across a broad diffuse plate boundary (denoted by grey in Fig. 1) that runs from the CIR near 5°S to the Java–Sumatra Trench near 100°E (Wiens *et al.* 1985; DeMets *et al.* 1988). Anomalies 31 to 34 lie within or north of this deformation zone. The portion of the Indian Plate south of this region of deformation was originally considered to form a distinct, separate Australian Plate. An additional diffuse plate boundary, active within the last 8 Ma or so, was later identified within the Australian Plate near the 90°E ridge (Royer & Gordon 1997). The portion of the Australian Plate west of that deformation zone was identified as a distinct rigid plate and referred to as the Capricorn Plate. Fortunately, the motion between the Indian Plate and the Capricorn Plate is well constrained by detailed magnetic studies along the Carlsberg and Central Indian Ridges (DeMets *et al.* 2005). The diffuse plate boundary between the Capricorn and Australian plates is more poorly constrained and we only use data on the SEIR from west of the 90°E ridge. Later in this paper we perform a test of the effect of the India–Capricorn deformation on the accuracy of the anomaly 34 to 31 SEIR rotations and show that it is relatively small.

The motion of India with respect to Africa is constrained by magnetic anomalies and fracture zones on the CIR (Norton & Sclater 1979; Patriat 1987). However, the complex series of tectonic events

Downloaded from https://academic.oup.com/gji/article/200/1/227/749250 by guest on 18 February 2022

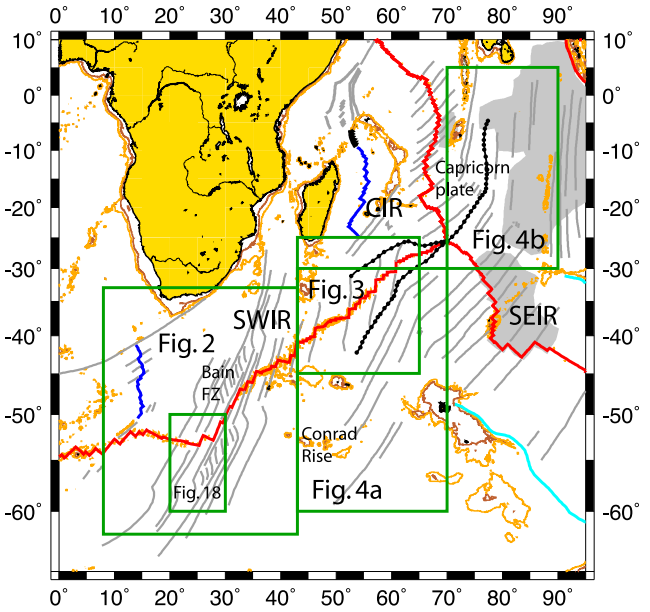


Figure 1. Tectonic elements of the Indian Ocean. Active spreading ridges are in red. Black chains demarcate triple junction traces. Grey shaded areas are zones of intraplate deformation.

between India and Madagascar that occurred around the time of the arrival of the Reunion plume head makes it difficult to accurately determine this history in detail. Spreading between India and Africa started with the rifting of India from Madagascar sometime before Chron 34y (Schlich 1982; Masson 1984). The most accurate record of the motion of India and Africa in the Late Cretaceous comes from the Mascarene Basin magnetic anomalies. Bernard & Munschy (2000) showed that spreading in the Mascarene Basin occurred in three stages: slow (40 mm yr^{-1}) from 34y to 33m, medium (80 mm yr^{-1}) from 33m to 31y and fast (160 mm yr^{-1}) from 31y to 28y. Eagles & Hoang (2013) have recently calculated a revised set of rotations for Africa–India motion from 84 until 45 Ma based on the magnetic anomalies and fracture zone data from the Mascarene Basin, Carlsberg ridge and the southwest flank of the CIR east of the Mascarene Basin using an innovative technique for constraining rotations where data only exist on a single side of the ridge.

Rifting between India and the Seychelles started in the Laxmi Basin and Gop Rift about the time of, or slightly pre-dating, the start of the Deccan traps (Bhattacharya *et al.* 1994; Minshull *et al.* 2008). Although there are linear magnetic anomalies in these basins which help constrain the start of this rifting, they are difficult to interpret because of the narrowness of the basins, leading to spreading models with conflicting ages. Bhattacharya *et al.* (1994) proposed that the Laxmi Basin anomalies formed by slow spreading between Chrons 33 and 28, while the Gop Rift anomalies have been variously attributed to spreading between Chrons 30 and 27 (Bernard & Munschy 2000), Chrons 32 and 31 (Collier *et al.* 2008), Chrons 31 and 25 or Chrons 29 and 25 (Yatheesh *et al.* 2009) or between Chrons 29 and 28 (Eagles & Wibisono 2013). Regardless of the differences in these interpretations, since spreading in the Mascarene Basin did not cease until Chron 27 (Dyment 1991; Bernard & Munschy 2000), there was a period of up to several million years when there was spreading both in the Mascarene Basin and along the southern continental margin of India leading to the development of the Seychelles microplate (Dyment 1991; Plummer 1996; Todal & Eldholm 1998; Royer *et al.* 2002; Cande *et al.* 2010; Eagles & Hoang 2013). The age of the onset of spreading on the Carlsberg Ridge is dated by magnetic anomaly 27 on the south side of the Laxmi Ridge and north slope of the Seychelles block and is attributed to a southward jump from the Gop Rift/Laxmi Basin (Collier *et al.* 2008; Armitage *et al.* 2011; Eagles & Wibisono 2013) between Chrons 28 and 27.

Cande *et al.* (2010) calculated 3-plate solutions for anomalies 13o to 29o in which the motions between Africa, Capricorn and Antarctica were solved simultaneously. Ideally, 3-plate solutions are more accurate and preferred to 2-plate solutions since more data are used in the solutions. Unfortunately, the geometry of the spreading centres in the Indian Ocean, specifically the limited spreading on the CIR outside of the Mascarene Basin, precludes the calculation of 3-plate solutions prior to anomaly 30 (Cande *et al.* 2010). Initially the focus of this study was to calculate 2-plate, pre-anomaly 30 rotations (31y to 34y), which would then be combined with the 3-plate, post-anomaly 30 rotations (29o to 20o), to form a detailed representation of Late Cretaceous through early Cenozoic motion. However, because the 2-plate SWIR solutions are not constrained by data from the CIR and SEIR, there potentially can be a small, artificially induced, jump in plate motion at the join of the 2-plate and 3-plate sets of SWIR rotations. Since this juncture, at anomaly 29, is a very critical point in the tectonic history, we preferred to have a set of SWIR solutions which are constrained by a uniform set of data. In addition, since we have redigitized some of the fracture zones on the SWIR and added some new magnetic anomaly constraints, the 3-plate solutions in Cande *et al.* (2010), particularly for the SWIR, are based on slightly different constraints than the 2-plate rotations presented here. Consequently, we have calculated 2-plate solutions for both the SWIR and SEIR for the entire interval from 34y to 20o. We sum the 2-plate SWIR and 2-plate SEIR rotations in order to calculate Capricorn–Africa (CIR) motion for the same interval.

3 DATA CONSTRAINTS

In this paper, we calculated a set of 12 rotations for the SWIR (for anomalies 34y, 33o, 33y, 32Ay, 31y, 28y, 26y, 24o, 23o, 22o, 21o and 20o) and a set of 17 rotations for the SEIR (for anomalies 34y, 33o, 33y, 32Ay, 31y, 29o, 28y, 27y, 26y, 25y, 24o, 23o, 22o, 21o, 21y, 20o and 20y) providing detailed records of plate motion changes in the Late Cretaceous and early Cenozoic. The ages of these anomalies are given in Table 1.

An index map of the region is shown in Fig. 1. The magnetic anomaly and fracture zone constraints for the SWIR are shown in Figs 2 and 3, while the data constraints for the SEIR are shown in Figs 4(a) and (b). The data constraints are from a mixture of sources. The primary data source for anomalies 29o and younger were the constraints used by Cande *et al.* (2010) while the data points for anomalies 34y to 31y mainly came from the Indian Ocean Data Compilation Project (Sclater *et al.* 1997). We superimposed these data constraints on plots of archival magnetic anomaly data and made new picks or altered old picks based on our appraisal. Magnetics data from two recent cruises to the SWIR not included in either of the two major sources were also analysed.

A challenging part of analysing SWIR plate motions is identifying the location of the fracture zone crossings on the Bain FZ complex around the time of the sharp clockwise bend near anomaly 24. As the satellite derived free-air gravity imagery (Fig. 5a) and fracture zone crossings (Fig. 5b) show, the fracture zone trends for anomalies 34y to 31y are clear and straightforward to map. However, as the change in direction becomes more acute, especially near anomalies 26y and 24o, the locations of the fracture zone crossings become more difficult to identify. In our previous work (Cande *et al.*

Downloaded from https://academic.oup.com/gji/article/200/1/227/749250 by guest on 18 February 2022

Table 1. Ages of magnetic anomalies.

Anom ID	Age (Ma)
13o	33.705
18o	40.145
20y	42.301
20o	43.432
21y	45.724
21o	47.349
22o	49.344
23o	51.833
24o	53.983
25y	57.101
26y	58.959
27y	62.221
28y	63.494
29o	65.688
31y	68.369
32Ay	71.449
32y	71.939
33y	74.309
33o	79.900
34y	83.640

Note: Ages are from GTS12.

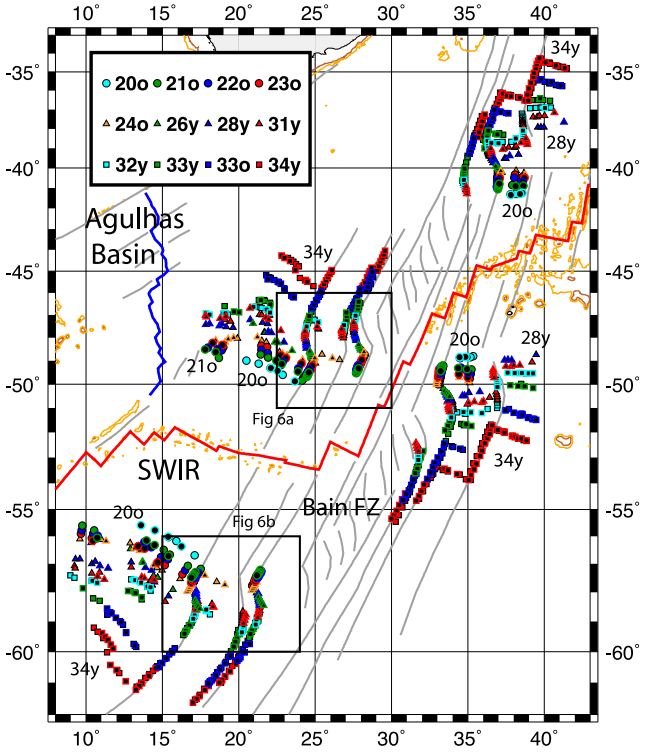


Figure 2. Magnetic anomaly picks and fracture zone locations from the western SWIR. Fixed points are shown with black rims and coloured cores, rotated points are shown with coloured rims and black cores.

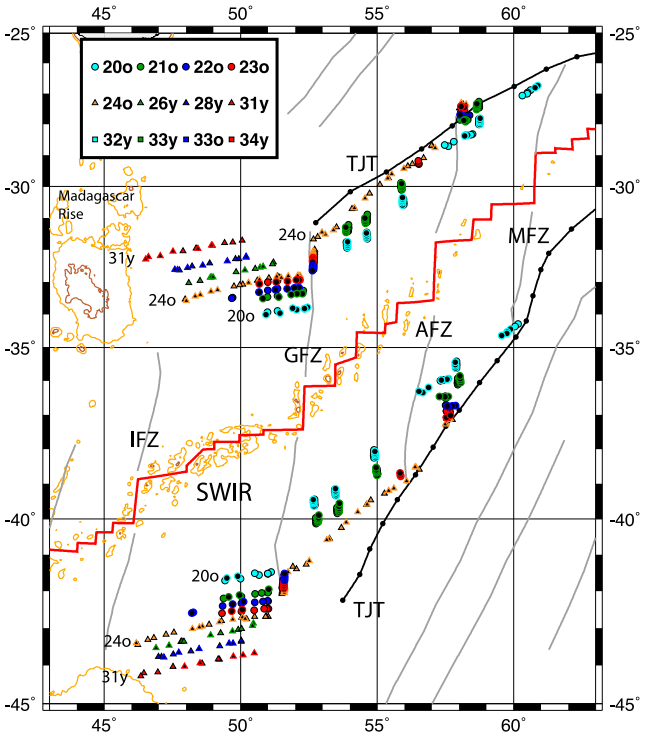


Figure 3. Magnetic anomaly picks and fracture zone locations from the eastern SWIR. IFZ, Indomed FZ; GFZ, Gallieni FZ; AFZ, Atlantis II FZ; MFZ, Melville FZ; TJT, Triple Junction Trace.

2010), we mapped the clockwise bend near anomaly 24 as a fairly smooth change in direction which took place over several million years. This was based on digitizing the gravity signal of five fracture zones (labelled 1–5 in Fig. 5b) including three splays (3, 4 and 5) that developed when the Bain FZ went into extension around Chron 32 and which disappeared shortly after Chron 24. However, upon re-examination of the gravity data we have decided that the controlling observation should be the abrupt nature of the clockwise bend on the two fracture zones west of the Bain FZ (1 and 2) and that the smooth nature of the clockwise bend in the central part of the Bain FZ complex might reflect the overprinting of the most acute part of the fracture zones, just before anomaly 24, by the prolonged period of north–south motion along the Bain following the clockwise bend. We note that Bernard *et al.* (2005) also interpreted the change in azimuth of the SWIR fracture zones around anomaly 24 as being very abrupt. Hence, for this study we only used three fracture zones, two from west of the Bain FZ (1 and 2) and one from east of the Bain FZ (labelled 6 in Fig. 5b), to define the fracture zone constraints at the time of the sharp clockwise bend near anomaly 24. Enlarged views of the satellite derived gravity field over the two fracture zones west of the Bain FZ (1 and 2) are shown in Figs 6(a) and (b) and our revised fracture zone crossings in Figs 6(c) and (d).

Constraints for most anomalies and fracture zones on the fast spreading SEIR are straightforward to identify. However, anomalies 34y, 33o and 33y on the Antarctic Plate in the southern Crozet Basin are more problematical because this area was later overprinted by the Conrad Rise (see Fig. 1 for location). Many of these magnetic anomaly picks are ambiguous, which lead to large uncertainty ellipses for these rotations. In addition, the constraints for SEIR anomalies 31y to 34y on the Indian Plate lie within or north of the deformation zone caused by convergence between the Indian and Capricorn plates (Fig. 4b, grey zone). This deformation could potentially have a large effect on the location of these data points. A full 3.22° rotation about the Chron 6 India–Capricorn rotation pole of DeMets *et al.* (2005) (5°S, 75°E) will shift a point near 85° E roughly 50 km to the north. However, since the deformation zone is broad and poorly mapped, the exact amount of displacement for any particular point is unknown. In order to evaluate the potential effect of the deformation on SEIR Euler rotations we calculated two additional rotations. In one, we corrected the anomaly 34y points

Downloaded from https://academic.oup.com/gji/article/200/1/227/749250 by guest on 18 February 2022

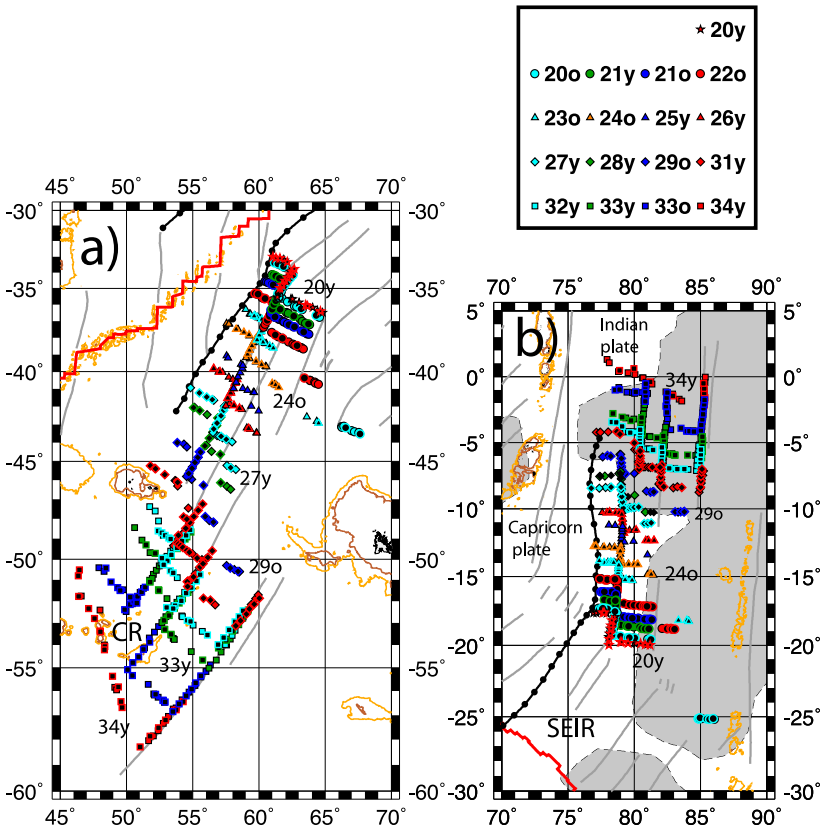


Figure 4. Magnetic anomaly picks and fracture zone locations used to constrain SEIR rotations. (a) Data from the Antarctic side of the SEIR. (b) Data from the Capricorn side of the SEIR. CR, Conrad Rise.

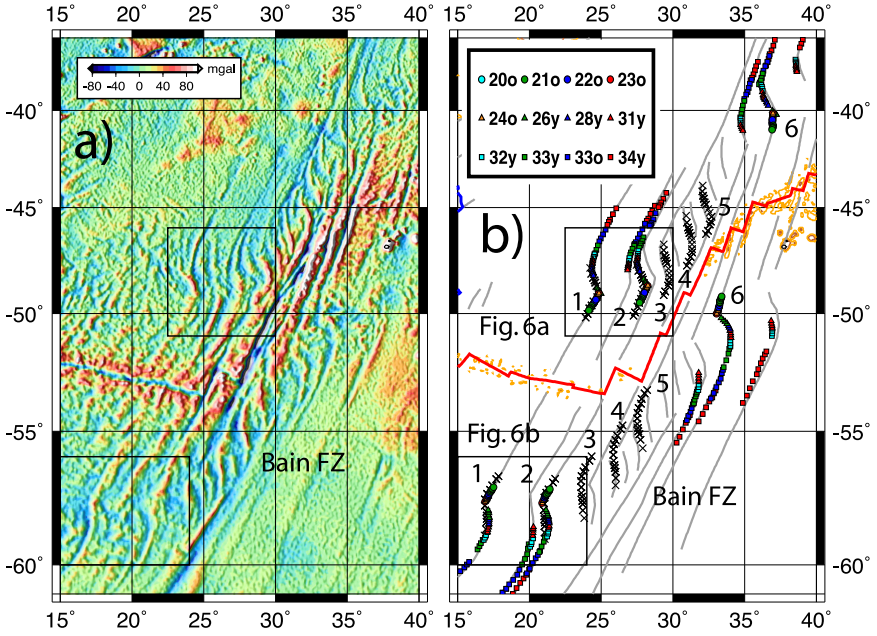


Figure 5. (a) Satellite derived free-air gravity anomalies (Sandwell & Smith 1997) over the region of the Bain FZ complex. (b) Comparison of the fracture zone locations used by Cande *et al.* (2010) (x's) to the fracture zone locations used in this paper (coloured symbols).

on the Indian Plate, which lie either north of or on the northern end of the deformation zone, by the full India–Capricorn deformation angle (3.22°). In the second test we corrected the Indian Plate SEIR constraints for anomaly 33y, which lie near the centre of the deformation zone, by 50 per cent of the Chron 6 India–Capricorn deformation angle (1.61°). We then calculated rotations using these corrected constraints and compared them to the rotations which did not include the correction for India–Capricorn deformation. The revised rotations fell within the uncertainty ellipses of the original rotations. We also calculated the effect of these alternative rotations

Downloaded from https://academic.oup.com/gji/article/200/1/227/749250 by guest on 18 February 2022

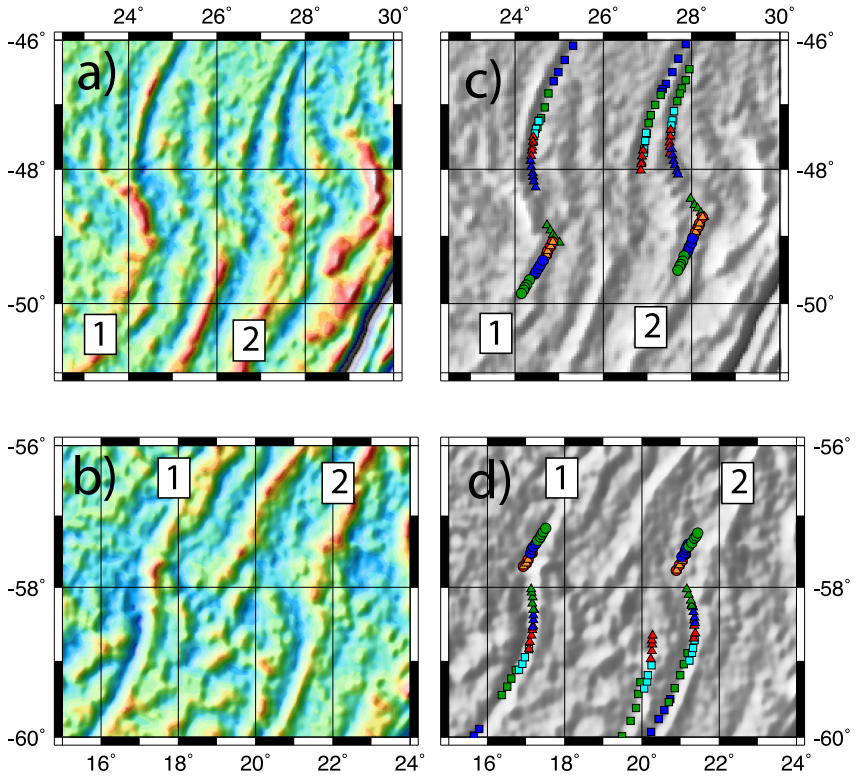


Figure 6. Enlargements of the satellite derived gravity field over (a) the African side and (b) the Antarctic side of the western SWIR showing the bends of the fracture zones west of the Bain FZ. The right-hand panels (c and d) show the fracture zone locations used in this paper. Colour scheme for symbols same as in Fig. 5(b).

on spreading rates along a flowline and found that the spreading rate averaged over the interval from 33y to 34y changed by roughly 2 mm yr^{-1} out of 77 mm yr^{-1}.

4 METHOD

We followed the method of Hellinger (1981) and determined rotation parameters by dividing the data into multiple segments and fitting great circles to the reconstructed data in each segment. The magnetic anomalies and fracture zones were used to define up to eight segments. We used the best-fitting criteria and statistical techniques of Chang (1987, 1988) and Royer & Chang (1991) to calculate rotation parameters and estimate uncertainty ellipses. This method requires that an estimate of the error in the position be assigned to every data point. Although it is possible to assign a separate error estimate to each data point, varying it, for example, for the type of navigation, this level of detail was beyond the scope of this study. Instead, based on our experience with other data sets, we generally assigned an estimate of 3 km for all magnetic anomaly points and 5 km for all fracture zone crossings. The quantitative method we used for fitting tectonic constraints requires that a minimum of three data points are present along any segment that is included in the solution (two on one flank of the ridge and one on the conjugate side). Hence only picks which met this requirement were used.

As part of the solution using the Chang (1987, 1988) method a statistical parameter, $\hat{\kappa}$, is returned which is an evaluation of the accuracy of the errors assigned to the location of the data points. If $\hat{\kappa}$ is near 1, the errors have been correctly assigned; if $\hat{\kappa}$ is $\gg 1$ the errors are overestimated; and if $\hat{\kappa}$ is $\ll 1$ the errors are underestimated. For most of our data sets, the value of $\hat{\kappa}$ was near 1, indicating that the error estimates were reasonable. For chrons where $\hat{\kappa}$ was greater than 1, the error values were overestimated by the $\sqrt{\hat{\kappa}}$, and for chrons were $\hat{\kappa}$ was less than 1, errors were underestimated by the $\sqrt{\hat{\kappa}}$. Although a $\hat{\kappa}$ of 1.0 could be obtained by dividing the original error estimates by $\sqrt{\hat{\kappa}}$, this rescaling makes no difference in the location of the poles and or in the size of the uncertainty ellipses. Consequently, for the sake of consistency, we cite the results using the original error estimates.

5 RESULTS

5.1 Africa–Antarctica rotations

Finite rotations for the SWIR based on the 2-plate solutions are presented in Table 2 and shown in Figs 7(a) and (b) with their 95 per cent uncertainty ellipses. In Fig. 7(a) we compare the new rotations (red triangles) to the 3-plate finite rotations of Cande *et al.* (2010) (blue triangles). For clarity we only show the Cande *et al.* (2010) rotations that correspond to the same anomalies as the new rotations (that is, we do not show their rotations for 29o, 21y and 20y). The new rotations deviate from the Cande *et al.* (2010) rotations everywhere except for anomaly 28y, reflecting the effect of using only two plates and the revised SWIR fracture zone and magnetic anomaly constraints. The youngest rotations (20o to 22o) are fairly close to the Cande *et al.* (2010) rotations and the differences mainly reflect minor changes in fracture zone constraints. The rotations for 23o, 24o and 26y diverge considerably from the Cande *et al.* (2010) solutions and reflect the large difference in mapping the sharp bend in the SWIR fracture zones before and after anomaly 24.

Downloaded from https://academic.oup.com/gji/article/200/1/227/749250 by guest on 18 February 2022

Table 2. Antarctica-Africa 2-plate finite rotations.

Anom	Lat. (°N)	Long. (°E)	Angle (°)	$\hat{\kappa}$	a	b	c	d	e	f	Points	Segs
20o	12.19	−41.44	7.90	0.88	5.23	4.52	4.72	−4.51	−4.45	5.17	75	9
21o	10.00	−40.66	8.83	1.18	2.33	1.85	2.21	−2.59	−2.63	4.27	95	12
22o	8.02	−39.67	9.19	1.29	2.22	1.30	1.63	−3.28	−2.78	6.89	69	9
23o	7.61	−39.30	9.63	0.83	4.99	3.12	3.21	−5.85	−4.45	9.56	66	9
24o	7.60	−39.57	9.98	0.54	1.95	1.56	1.77	−1.55	−1.88	2.93	104	15
26y	6.69	−42.74	10.58	1.51	19.80	19.86	20.96	−20.79	−20.88	25.79	46	5
28y	3.81	−43.67	11.17	0.60	6.17	5.74	6.42	−9.86	−9.61	18.52	61	8
31y	0.64	−43.29	11.98	0.33	4.04	2.61	2.29	−5.82	−3.96	10.15	95	12
32Ay	−3.27	−41.14	12.83	1.16	7.44	3.15	1.82	−10.99	−4.82	18.58	83	11
33y	−5.38	−39.54	13.91	0.94	12.38	5.22	3.21	−19.64	−9.15	33.90	67	9
33o	−3.27	−39.79	15.98	1.14	7.99	3.68	2.21	−13.28	−6.41	23.63	91	9
34y	−1.35	−39.52	17.82	0.50	5.97	3.19	2.08	−10.07	−5.63	18.21	122	10

Notes: a, b, c, d, e, and f are covariances and have units of 10^{-7} radians^2.
Covariance matrices are reconstructed from the equation

$$\frac{1}{\hat{\kappa}} \times \begin{pmatrix} a & b & d \\ b & c & e \\ d & e & f \end{pmatrix}.$$

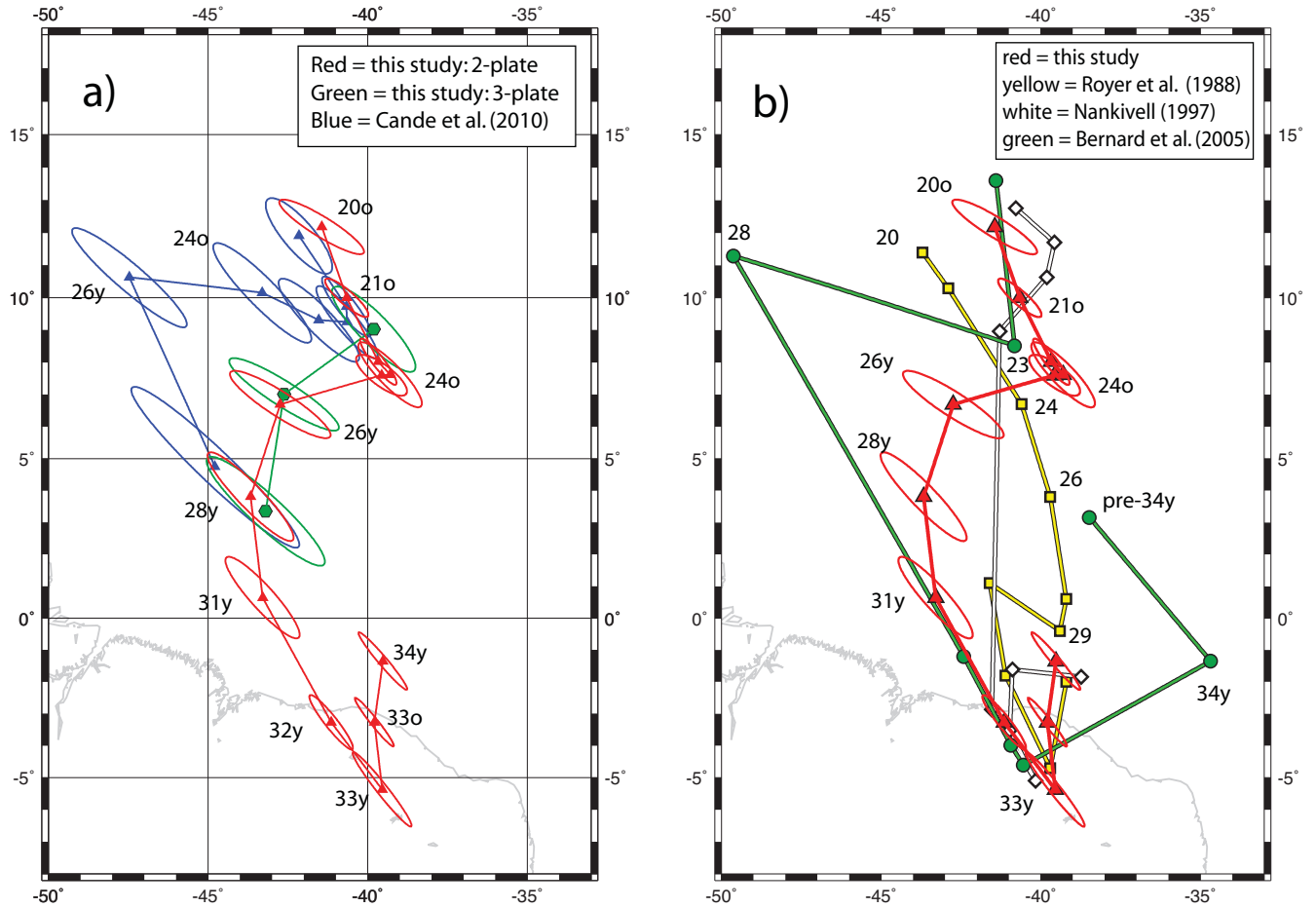


Figure 7. (a) Revised 2-plate finite rotation poles for the SWIR (red triangles) compared to 3-plate finite rotation poles from Cande *et al.* (2010) (blue triangles) and revised 3-plate finite rotation poles from this study (green hexagons). Ellipses show 95 per cent confidence boundaries. (b) Revised 2-plate finite rotation poles for the SWIR (red triangles) compared to finite rotation poles from Royer *et al.* (1988) (yellow squares), Nankivell (1997) (white diamonds) and Bernard *et al.* (2005) (green circles).

In order to discriminate between the effect of using the revised fracture zone and magnetic anomaly constraints and the effect of using 2-plate versus the larger set of 3-plate constraints, we also recalculated 3-plate solutions (Kirkwood *et al.* 1999) for Cap–Ant–Afr motion for anomalies 24o, 26y and 28y, using the same constraints as in Cande *et al.* (2010), except substituting the revised fracture zone and magnetic anomaly picks on the SWIR that we used here for Ant–Afr motion. The revised 3-plate SWIR rotations are given in Table 3 and shown in Fig. 7(a) (green hexagons). These revised rotations constrained by 3-plates fall close to our new 2-plate

Downloaded from https://academic.oup.com/gji/article/200/1/227/749250 by guest on 18 February 2022

Table 3. Antarctica–Capricorn 2-plate finite rotations.

Anom	Lat. (°N)	Long. (°E)	Angle (°)	$\hat{\kappa}$	a	b	c	d	e	f	Points	Segs
20y	17.59	28.05	24.32	0.68	187.38	368.92	730.71	–292.16	–576.81	458.93	28	3
20o	16.85	27.99	25.17	0.78	19.81	40.83	88.07	–33.00	–69.02	57.51	39	4
21y	17.32	25.93	26.26	1.35	202.09	376.67	706.78	–311.06	–580.36	481.26	30	3
21o	14.67	27.07	28.11	3.99	175.89	332.52	632.17	–274.74	–520.39	431.18	38	3
22o	15.35	23.82	29.30	2.01	133.82	243.69	448.75	–210.17	–383.20	332.95	42	4
23o	13.74	22.98	32.07	1.15	58.08	103.12	186.51	–92.35	–164.56	148.80	35	4
24o	12.94	22.13	34.58	2.48	147.75	255.99	447.57	–239.15	–415.06	389.55	31	4
25y	12.96	18.91	37.36	2.17	790.25	1280.67	2079.79	–1267.31	–2055.67	2036.40	26	4
26y	11.77	18.89	39.64	2.16	393.01	637.10	1038.67	–655.75	–1065.72	1099.07	25	4
27y	9.91	18.41	43.59	3.47	219.60	340.32	530.68	–371.57	–576.55	631.80	27	4
28y	9.31	17.92	45.45	1.49	1147.95	1667.75	2430.09	–1890.14	–2751.64	3121.38	20	4
29o	10.57	14.13	47.84	1.21	69.47	108.34	172.69	–135.47	–212.55	268.26	27	5
31y	10.56	12.37	51.26	0.38	90.03	126.08	178.75	–182.48	–257.48	373.61	60	7
32Ay	9.69	12.46	54.21	0.14	71.76	99.94	141.22	–149.63	–210.08	314.82	58	6
33y	9.07	12.79	56.56	0.33	79.05	105.42	144.43	–165.91	–223.05	351.31	53	6
33o	10.52	9.73	60.03	0.31	36.42	45.46	58.63	–78.23	–99.13	171.09	55	5
34y	9.49	10.56	63.88	0.04	90.77	97.33	109.99	–191.95	–210.54	412.21	32	4

rotations and show that the differences between the Cande *et al.* (2010) and the new rotations are primarily driven by the revised data constraints.

In Fig. 7(b) we compare our new 2-plate rotations (red triangles) to the rotations of Royer *et al.* (1988) (yellow squares), Nankivell (1997) (white diamonds) and Bernard *et al.* (2005) (green circles). Fig. 7 shows that over much of the time there are considerable differences in the rotations for all of the solutions. Our rotation for anomaly 34y is very close to Nankivell (1997) and Royer *et al.* (1988) but all three diverge from Bernard *et al.* (2005). Our new rotation for 33y agrees well with Royer *et al.* (1988) although there are small differences with Nankivell (1997) and Bernard *et al.* (2005). However, going forward in time the solutions diverge considerably showing the difficulty of interpreting the younger fracture zones and anomalies.

Our new rotations map out a distinctly different path for the migration of the finite rotation poles than the previous solutions. The effect of the differences in the rotations is seen in a comparison of synthetic flowlines modelling the bends of the SWIR fracture zones shown in Fig. 8. Synthetic flowlines based on our new rotations (yellow circles) define the clockwise bend at anomaly 24 as a much sharper bend than the flowlines based on Cande *et al.* (2010) (red triangles), reflecting the revised fracture zone constraints used in the new solutions.

The new rotations constrain several changes in plate motion on the SWIR between Chrons 34 and 24. This is best seen in the path of the stage poles, plotted with respect to Africa fixed, shown in Fig. 9. Between Chrons 34y and 33y the stage poles are roughly stationary. Between Chrons 33y and 31y the stage poles migrate to the southeast, after which they make an abrupt change and migrate to the west–northwest, and then, after Chron 24o, there is an abrupt shift in the stage poles back to their location in the Late Cretaceous. We will discuss the possible causes of these changes in motion later.

5.2 Capricorn–Antarctica rotations

In Table 4 we present finite rotations for the SEIR. These rotations (red triangles), with their uncertainty ellipses, are shown in Fig. 10 and compared to the SEIR rotations of Royer & Sandwell (1989) (yellow squares), and Cande *et al.* (2010) (blue triangles). The rotations do not deviate significantly from the previous rotations, but represent a more detailed set of time steps. The uncertainty ellipses

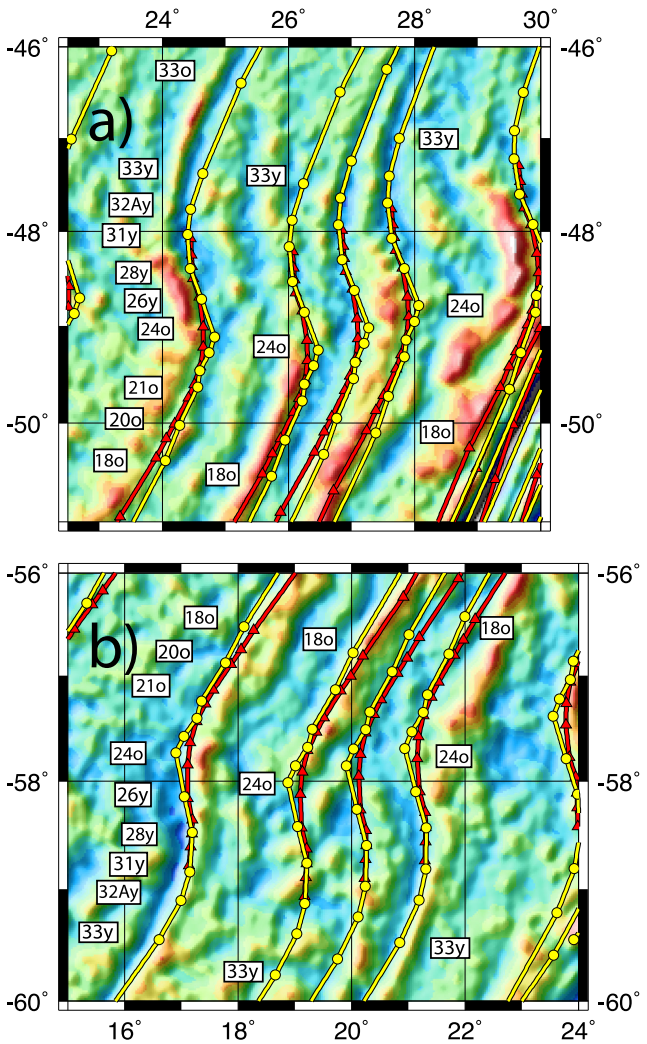


Figure 8. Synthetic flowlines for (a) the African side and (b) the Antarctic side of the western SWIR based on the revised SWIR rotations (yellow circles) compared to flowlines based on rotations of Cande *et al.* (2010) (red triangles). Revised rotations define a sharper clockwise bend at Chron 24o. Flowlines are superimposed on gravity anomalies constrained by satellite altimetry data.

Downloaded from https://academic.oup.com/gji/article/200/1/227/749250 by guest on 18 February 2022

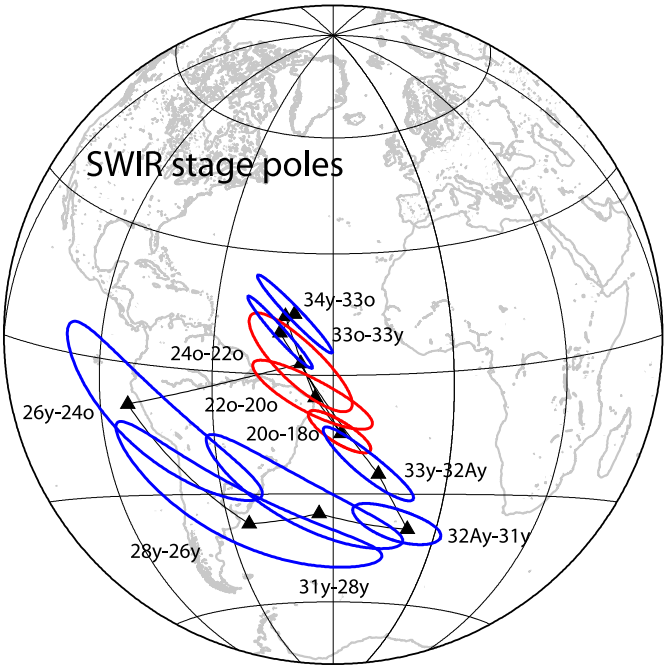


Figure 9. Stage poles with their 95 per cent uncertainty ellipses for Afr–Ant motion based on the revised 2-plate finite rotation poles shown in Figs 7(a) and (b). For clarity, the uncertainty ellipses for 34y-33o to 26y-24o are in blue; the ellipses for 24o-22o to 20o-18o are in red. The stage poles define three periods in the motion of the SWIR: the period from 33y to 31y when the stage poles migrate to the southeast, the period from 31y to 24o when the stage poles migrate to the northwest, and the period after 24o when the stage poles move back to the east. African plate is fixed.

Table 4. Antarctica–Africa 3-plate finite rotations.

Anom	Lat. (°N)	Long. (°E)	Angle (°)	$\hat{\kappa}$	a	b	c	d	e	f	Points	Segs
24o	9.03	−39.81	9.97	0.66	4.21	3.00	3.11	−5.39	−4.20	9.00	141	17
26y	7.01	−42.62	10.57	1.87	17.94	18.47	20.26	−19.18	−19.93	23.78	90	11
28y	3.36	−43.20	11.19	0.74	8.29	8.73	10.35	−12.39	−13.78	22.27	100	13

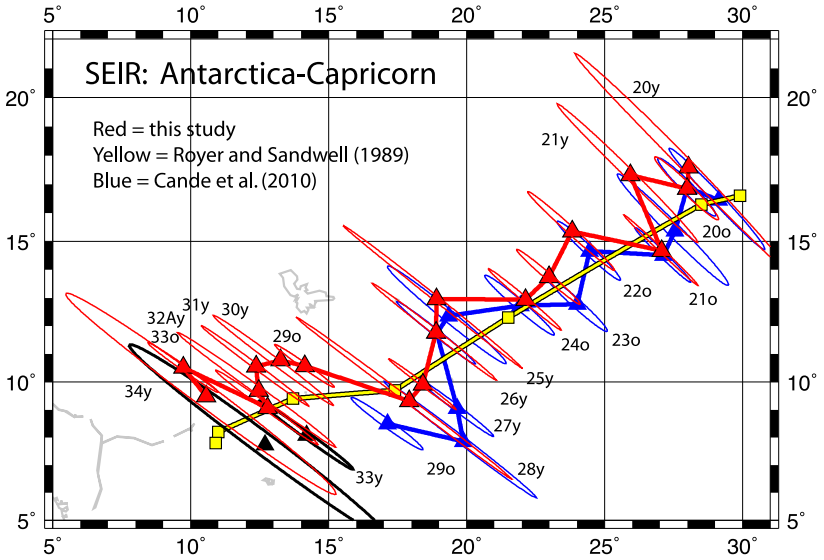


Figure 10. Revised 2-plate finite rotations poles for the SEIR (red triangles) compared to 3-plate finite poles from Cande *et al.* (2010) (blue triangles), and 2-plate finite poles of Royer & Sandwell (1989) (yellow squares). Black triangles show location of alternate finite rotation poles for anomalies 34y and 33y in which the data constraints on the Capricorn Plate were corrected for Neogene India-Capricorn deformation. See text.

were particularly large for anomalies 33y and 34y, reflecting the difficulty in mapping anomalies near the Conrad Rise in the Crozet Basin where there are few magnetic lines that are not obviously affected by rough topography (Desa *et al.* 2009). The uncertainties for all of the SEIR rotations are generally large, reflecting the relatively short length of the ridge over which they are constrained.

In Fig. 10, we also show the pole locations for the two additional rotations described in the Data Constraints section in which we

Downloaded from https://academic.oup.com/gji/article/200/1/227/749250 by guest on 18 February 2022

Table 5. Africa–Capricorn summed and interpolated finite rotations.

Anom	Lat. (°N)	Long. (°E)	Angle (°)	$\hat{\kappa}$	*a*	*b*	*c*	*d*	*e*	*f*	SWIR	SEIR
20o	17.92	47.20	23.24	0.84	28.47	52.97	109.74	−32.77	−65.15	42.29	x	x
21o	16.88	46.03	25.80	1.49	209.81	399.28	767.30	−237.24	−453.18	270.94	x	x
22o	18.77	42.51	26.31	1.50	164.53	298.53	551.43	−184.41	−334.93	210.29	x	x
23o	17.49	40.53	28.69	0.92	77.29	131.85	236.21	−85.23	−147.37	97.65	x	x
24o	16.85	38.76	30.93	0.66	186.20	323.25	567.64	−208.74	−364.05	237.67	x	x
25y	17.33	34.62	33.33	1.00	472.55	762.64	1235.55	−517.14	−836.69	569.30		x
26y	16.21	33.93	35.67	1.66	541.53	857.30	1371.31	−604.34	−963.30	684.47	x	x
27y	14.98	32.27	39.48	1.00	95.75	140.48	210.25	−107.23	−157.72	122.64		x
28y	14.62	31.22	41.22	0.67	1598.58	2269.92	3232.97	−1738.95	−2472.96	1898.98	x	x
29o	16.59	26.55	42.75	1.00	94.73	135.78	201.59	−118.26	−170.93	151.58		x
31y	17.17	23.82	45.62	0.35	148.60	195.20	261.19	−190.99	−253.11	249.08	x	x
32Ay	17.51	23.17	47.92	0.28	131.45	163.66	212.16	−165.58	−209.12	212.02	x	x
33y	17.88	23.36	49.59	0.51	157.50	184.17	227.48	−192.33	−228.32	238.30	x	x
33o	18.74	22.68	52.61	1.00	1531.41	1729.30	2009.40	−1819.22	−2076.81	2182.44	x	
34y	19.36	22.66	54.28	0.17	182.38	196.53	219.56	−206.74	−225.79	237.29	x	x

corrected for the effect of India–Capricorn deformation on the location of the anomaly 33y and 34y picks on the Indian Plate. These two rotations (black triangles) both fall within the uncertainty ellipses of the rotations using constraints that have not been corrected for India–Capricorn deformation. We calculated the effect these alternate rotations would have on the spreading rates we present in the next section and found that the effect was very small, roughly 2 mm yr^{-1} during a period when the total rate was on the order of 100 mm yr^{-1}. Consequently, we did not use these rotations further.

5.3 Capricorn–Africa rotations

We calculated finite rotations for the CIR (Capricorn–Africa) by summing our revised Capricorn–Antarctica and Antarctica–Africa 2-plate finite rotations. The new CIR rotations are given in Table 5. In Fig. 11 we compare the new rotations (red triangles) to the 3-plate finite rotations of Cande *et al.* (2010) (blue triangles = 'no Carlsberg ridge' constraints; black triangles = 'with Carlsberg ridge' constraints), the 2-plate finite rotations of Royer *et al.* (2002) (yellow squares) and the finite rotations of Eagles & Hoang (2013) (green stars). Because the Eagles & Hoang (2013) rotations are for India–Africa, we summed them with the DeMets *et al.* (2005) Chron 6 Capricorn–India rotation to get a more comparable Capricorn–Africa rotation. We note that between anomalies 22o and 29o our new CIR rotations are systematically offset about 200 km to the north of the Cande *et al.* (2010) 3-plate rotations computed with no Carlsberg ridge constraints (blue triangles) and between anomalies 22o and 25y are in agreement with the Cande *et al.* (2010) 3-plate rotations which included Carlsberg constraints (black triangles). Cande *et al.* (2010) argued that the difference in the 3-plate rotations with and without Carlsberg ridge constraints prior to anomaly 22o supported the existence of a separate Seychelles microplate as young as anomaly 23o. However, the better agreement between our new CIR rotations and the 3-plate rotations of Cande *et al.* (2010) using Carlsberg constraints suggests that the Seychelles microplate ended earlier than Chron 25y. This is in agreement with the results of Eagles & Hoang (2013) who found that the Seychelles microplate ended around Chron 27.

6 REVISED SPREADING RATES

We calculated spreading rates along three representative trajectories (Fig. 12) crossing the SEIR (Cap–Ant), SWIR (Afr–Ant) and CIR (Cap–Afr) using the revised rotations in Tables 2 and 4. For time

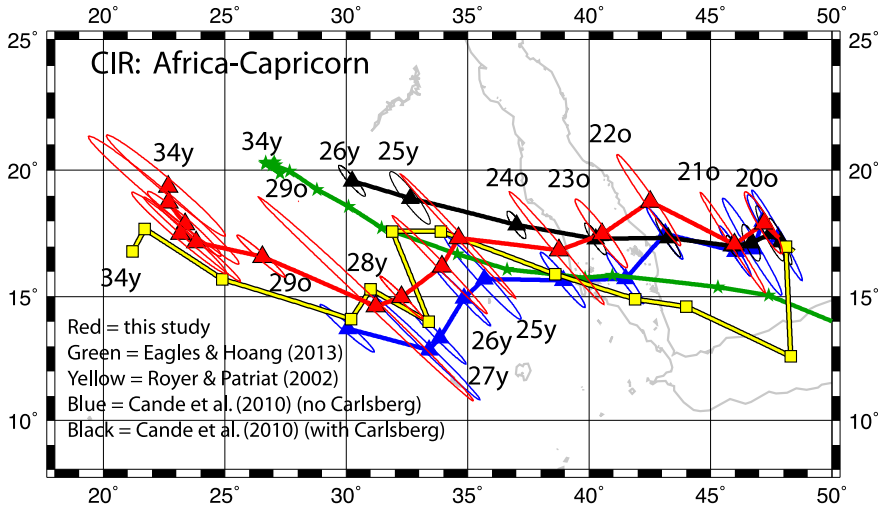


Figure 11. Finite rotation poles for the CIR (red triangles) based on summing the revised finite rotations for the SEIR and SWIR compared to two different sets of 3-plate finite rotation poles from Cande *et al.* (2010) (blue triangles and black triangles). Also shown are the 2-plate finite poles of Royer & Patriat (2002) (yellow squares) and the 2-plate finite poles of Eagles & Hoang (2013) (green stars).

Downloaded from https://academic.oup.com/gji/article/200/1/227/749250 by guest on 18 February 2022

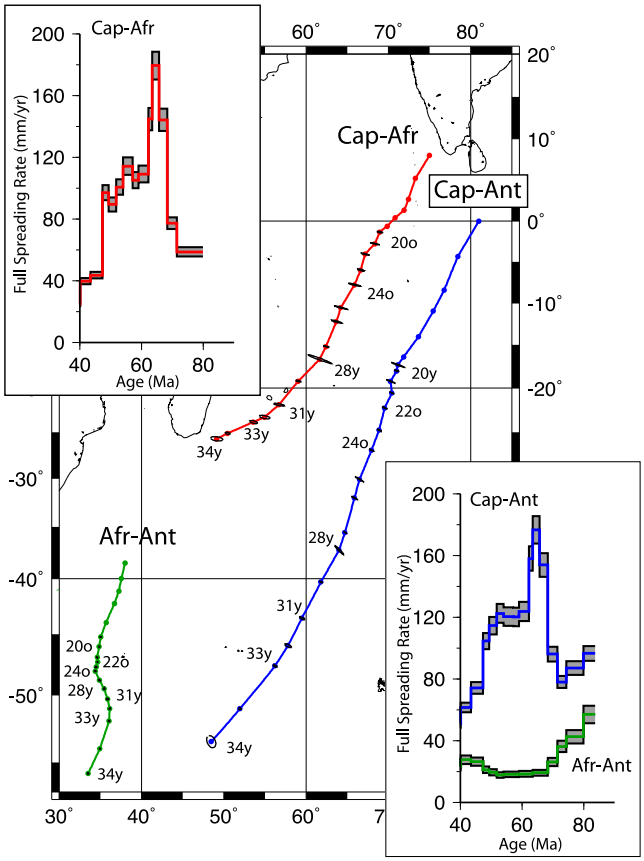


Figure 12. Trajectories for three representative points, one each on the SEIR (Cap–Ant; blue), SWIR (Afr–Ant; green) and CIR (Cap–Afr; red). Ellipses show 95 per cent confidence zones for the rotated points. Insets show spreading rates along the trajectories using the GTS12 timescale with an estimate of the error based on the confidence zones.

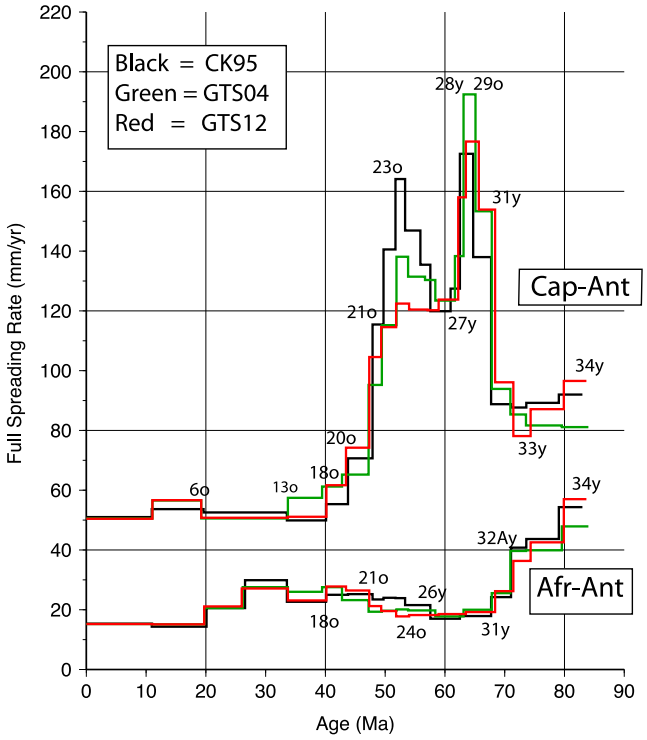


Figure 13. Effect of recent changes to the geomagnetic polarity timescale on spreading rates. Top panel: three profiles show comparison of spreading rates on the SEIR (Cap–Ant) based on the timescales of CK95 (black), GTS04 (green) and GTS12 (red). Bottom panel: three profiles show effect of the same timescale changes on spreading rates on the SWIR (Afr–Ant).

intervals younger than Chron 20 we used rotations from Cande *et al.* (2010) (Chrons 18o and 13o), Patriat *et al.* (2008) (SWIR: Chrons 8o and 6o), Lemaux *et al.* (2002) (SWIR: Chron 5o), Molnar *et al.* (1988) (SEIR: Chrons 6m and 5o) and DeMets *et al.* (2005) (CIR: Chrons 6o and 5o). In Fig. 12 we also show 95 per cent confidence zones for the position along the trajectories at Chrons 20y to 34y based on the covariance matrices. Because of the large size and close spacing of a few of the 95 per cent confidence zones we decided not to show spreading rates on the CIR for Chrons 34y and 33y and on the SEIR for anomalies 20y and 21y. In the insets in Fig. 12 we show an estimate of the errors in spreading rates on the three trajectories that can be attributed to the errors in the finite rotations using the GTS12 timescale. The errors for the time intervals we show in the following figures are less than 5 per cent.

Since recent changes to the geomagnetic polarity timescale have induced significant changes to the plate velocities, we have calculated the spreading rates for the SWIR and SEIR (Fig. 13) using three timescales: Cande & Kent (1995) {CK95}, Gradstein *et al.* (2004) {GTS04} and Ogg (2012) {GTS12}. On the fast spreading SEIR (Cap–Ant), the changes are large and have the potential of changing the perception of the importance of various tectonic events. With CK95 there is a rapid increase in spreading rate starting around Chron 31y, a period of superfast spreading (180 mm yr^{-1}) between Chrons 29o and 28y, a rapid drop to 120 mm yr^{-1} between Chrons 28y and 27y, a second period of faster spreading (160 m yr^{-1}) centred on Chron 24, and a prolonged slowdown that runs from 23o until Chron 18o, with the fastest slowing centred on Chron 20. With GTS04 the maximum rate between Chrons 29o and 28y is a little faster (200 mm yr^{-1} instead of 180), the rate also falls off rapidly to about 120 mm yr^{-1} by Chron 27y, there is still a secondary speedup, but smaller, centred on Chron 24, and a long period of slowing from 23o until 18o with the fastest slowing centred on Chron 21. With GTS12 the fastest rate (between Chrons 29o and 28y) is, as in CK95, about180 mm yr^{-1} and there is still a rapid drop between Chrons 28y and 27y. Significantly, however, there is only a very small secondary speedup around Chron 24 and the moderate rate of slowing, which started around Chron 27y, continues relatively uniformly until Chron 21o after which the rate falls off rapidly.

The effect of the changes in the timescale are smaller on the slow spreading SWIR (Afr–Ant), but not entirely insignificant (Fig. 13). With CK95 and GTS04 there is a relatively abrupt drop in spreading rates around Chron 32Ay (71 Ma). With GTS12 the abrupt nature of this drop is diminished and there appears to be a more continuous drop off in spreading rate between Chron 34y and 31y. We note that spreading rates on the SEIR (Cap–Ant) between Chrons 32Ay and 33y are more irregular with GTS12 than with CK95 or GTS04, suggesting that there may still be significant problems with the GPTS around Chron 32.

In Fig. 14, we compare spreading rates for all three sets of rotations presented in this paper (the SEIR, SWIR and CIR) plus spreading rates calculated for South America–Africa (Sam–Afr) as constrained by the rotations of Müller *et al.* (1999). In the left-hand panel of Fig. 14 we show the spreading rates using GTS04 while in the right-hand panel we show the spreading rates based on GTS12. Because of the relatively large errors in the Cap–Afr rotations for Chrons 34y and 33y we only calculated an average spreading rate between Chrons 33o and Chron 32Ay, and no spreading rate prior to

Downloaded from https://academic.oup.com/gji/article/200/1/227/749250 by guest on 18 February 2022

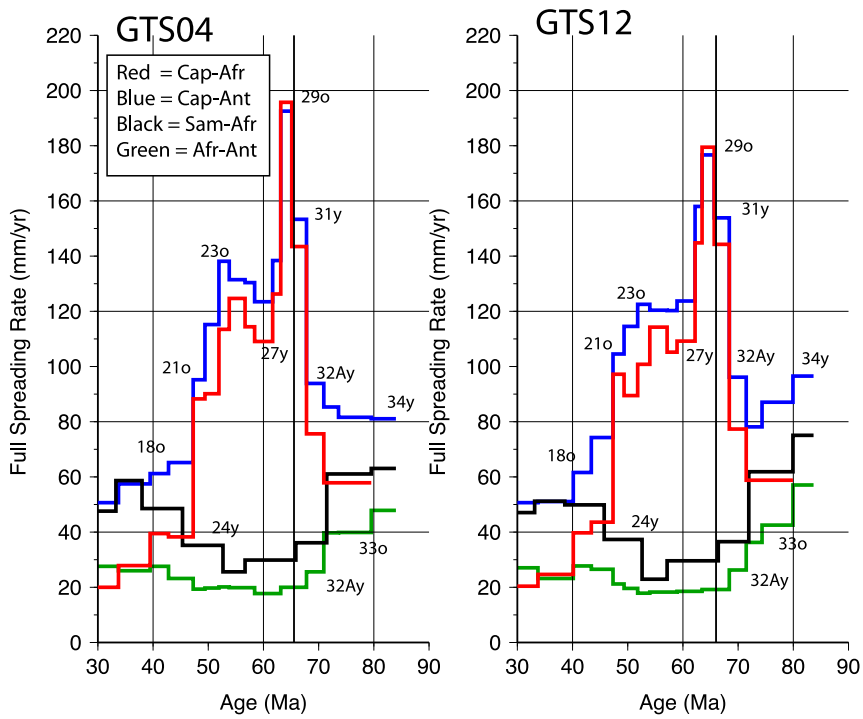


Figure 14. Comparison of relative spreading rates on the SEIR (blue), CIR (red), SWIR (green) and Southern MAR (black) for two geomagnetic polarity timescales: GTS04 (left-hand side) and GTS12 (right-hand side). With both timescales the major drop in spreading rates on the SWIR and Southern MAR occur around Chron 32Ay (71 Ma) while the major speedup on the CIR and SEIR occurs after Chron 31y (68 Ma). Vertical black line shows Cretaceous/Tertiary boundary.

Chron 33o. However, Chron 32Ay (71 Ma) clearly marks an acceleration in Cap–Ant spreading, may mark an acceleration in Cap–Afr rates and is synchronous with a sharp drop in Sam–Afr rate in both GTS04 and GTS12. Chron 32Ay also marks the time of a drop in Afr–Ant rates, although this is more pronounced in GTS04 than in GTS12. The end of the period of superfast spreading, marked by the rapid fall in rates on Cap–Ant and Cap–Afr around Chron 27, corresponds to no significant changes in rates on Afr–Ant and Afr–Sam. The sudden shift in the position of the Afr–Ant (SWIR) stage poles back to the east around Chron 24 corresponds to a large increase in spreading rate in the South Atlantic (Afr–Sam) but to only very minor changes in rate on any of the other ridges. We note that the more continuous fall off in Cap–Ant spreading rates between 27y and 21o in GTS12 than in GTS04 (that is, the lack of an increase in velocities near Chron 24) is also apparent in Cap–Afr rates. The more precipitous drop in Cap–Ant rates at Chron 21o in GTS12 is also apparent in Cap–Afr rates.

6.1 Absolute plate velocities

Changes in the velocity of the Indian and African plates relative to the mantle follow fairly closely changes in the relative velocities of Cap–Afr and Afr–Ant, respectively. This is demonstrated in Fig. 15 where we show the results of summing our revised Cap–Afr rotations with the Afr–Abs rotations of Müller *et al.* (1993). The ensuing Cap–Abs rotations were used to calculate the velocity of India (Cap) along the same flowline as shown for the velocity of Cap–Afr (that is, ending at 8°N, 75°E). We also compare the velocity of Afr–Abs to the velocity of Afr–Ant for the flowline in Fig. 12 (ending at 38°S, 38°E). For both Afr–Abs and Cap–Abs the changes in velocities along the flowlines closely follow the changes in the Afr–Ant and Cap–Afr spreading rates, demonstrating that changes in the relative spreading rates are a good proxy for changes in the absolute motions. The velocity of India with respect to the mantle is roughly 20–30 mm yr^{-1} faster than the velocity of Cap–Afr spreading throughout this period.

6.2 Fine tuning Chron 29

Individual marine magnetic profiles provide a more detailed record of the changes in spreading rate during the period of superfast spreading around Chrons 29 and 28. Cande & Stegman (2011) showed that with the GTS04 timescale two ship profiles, one from the Mascarene Basin (CIR) and the other a composite profile compiled from conjugate flanks of the SEIR, displayed the fastest spreading rate during Chron 29N. However, a plot of spreading rates between Chrons 27 and 31 on profiles from the Pacific-Farallon (Pac-Far) ridge using the GTS04 timescale displayed large fluctuations in rates indicating that the timescale was inaccurate near Chrons 29N/29R. In order to smooth out the fluctuations in Pac-Far spreading rates, 120 kyr had to be added to Chron 29N and subtracted from Chron 29R. When this timescale modification was applied to the SEIR and CIR profiles it was apparent that the fastest spreading was within Chron 29R, the time of the most effusive outpouring of Deccan Basalts (Chenet *et al.* 2007). We repeated the same test with GTS12 and found that without any changes to the timescale the Pac-Far profiles still had large fluctuations in spreading rate between Chrons 29N and 29R (left-hand side, Fig. 16). By adding 80 kyr to 29N and subtracting 80 kyr from 29R the Pac-Far spreading rates were smoothed out (right-hand side, Fig. 16). Applying the same correction to two profiles from the SEIR, one based on our revised rotations (blue) and a second based on the same composite ship profile (red) used in Cande & Stegman (2011), shows that the fastest Cap–Ant spreading occurred within Chron 29R and

Downloaded from https://academic.oup.com/gji/article/200/1/227/749250 by guest on 18 February 2022

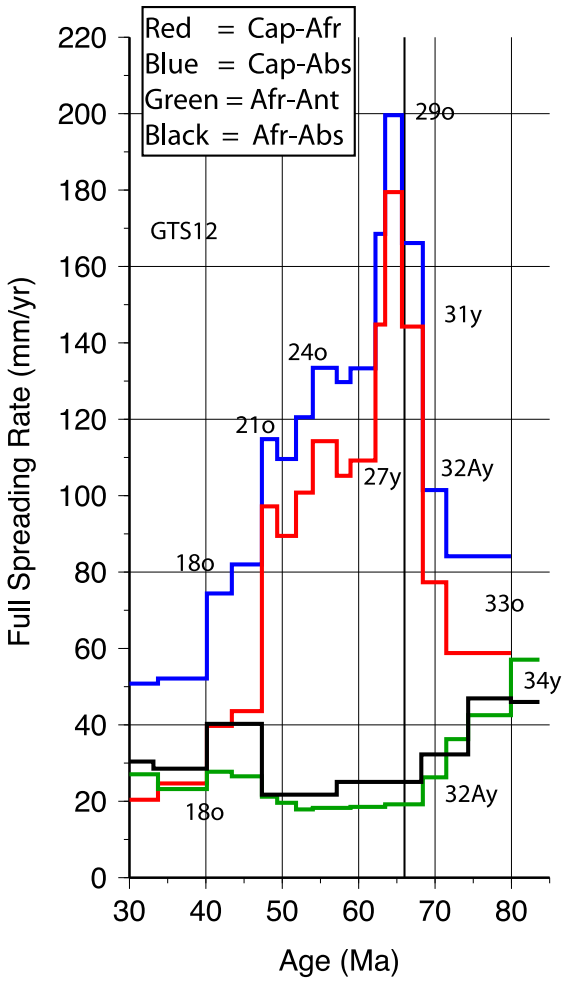


Figure 15. Comparison of the absolute velocities of the Capricorn (Cap–Abs; blue) and African (Afr–Abs; black) plates to the relative spreading rates on the CIR (Cap–Afr; red) and SWIR (Afr–Ant; green) using the GTS12 timescale.

was nearly 200 mm yr^{-1}. Based on our observation (Fig. 15) that the absolute velocity of India was roughly 20–30 mm yr^{-1} faster than the Cap–Afr spreading rate, we estimate that the absolute velocity of India during Chron 29R was about 220 mm yr^{-1}.

6.3 Mascarene basin constraints

Spreading rates based on magnetic anomalies from the Mascarene Basin (Eagles & Hoang 2013) give a slightly different spreading history for Cap–Afr motion than that predicted by summing our new rotations for Cap–Ant and Ant–Afr. In Fig. 17 we compare spreading rates for the representative Cap–Afr trajectory shown in Fig. 12 using our revised CIR rotations and the rotations recently determined by Eagles & Hoang (2013). The profile based on the Eagles & Hoang (2013) rotations (green) has a much narrower spike of superfast spreading confined almost entirely to Chron 28R and 29N than the spreading rate history based on the our revised CIR rotations (red). It is not clear if this result is due to (1) a missing plate boundary or zone of plate deformation not adequately accounted for with our revised Cap–Ant and Ant–Afr rotations (e.g. unrecognized motion between the Nubia and Somalia Plate in the early Cenozoic), (2) motion between the Seychelles microplate and India not adequately accounted for in the Eagles & Hoang (2013) model or (3) inadequate (not representative) coverage in the Mascarene Basin in the Eagles & Hoang (2013) study. Resolving this discrepancy is an important issue for future studies.

7 DISCUSSION

Our revised rotations enable us to speculate about whether the changes in the motion of India and Africa in the Late Cretaceous and early Cenozoic were driven by a plume head push. We note that the overall shape, if not the amplitude, of the Cap–Afr spreading rate profile is similar to the prediction of the simple plume head model of van Hinsbergen *et al.* (2011) from Chron 33o (80 Ma) to Chron 21o (47 Ma), a period of over 30 Ma. There is an initial moderate rise in spreading rate between Chrons 32Ay and 31y,

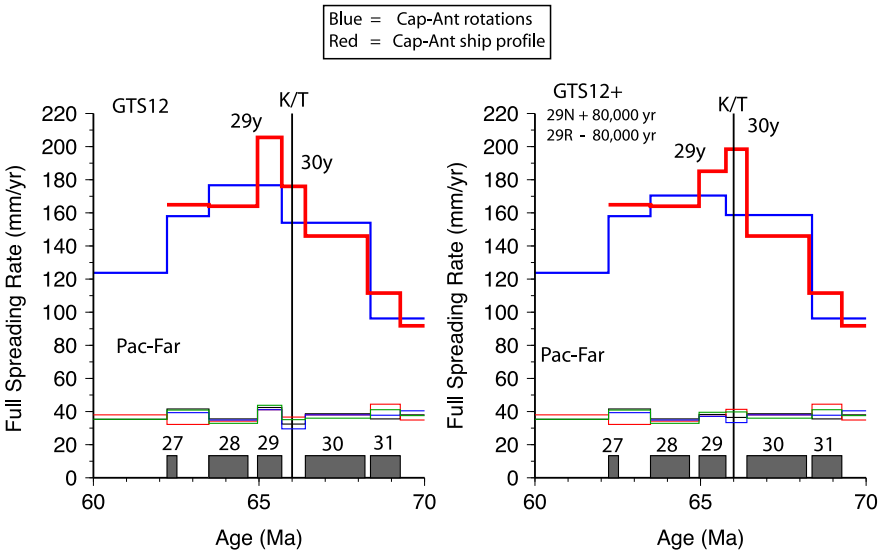


Figure 16. Demonstration of the effect of problematical polarity durations within Chron 29 on the motion of India. Pacific-Farallon (Pac-Far) spreading rates based on single ship profiles using GTS12 (left-hand side) have large fluctuations within Chron 29 that are eliminated (right-hand side) by adding 80 kyr to Chron 29N and subtracting 80 kyr from Chron 29R. The same correction when applied to Cap–Ant spreading rates based on (1) a composite single ship profile (red) and (2) on our 2-plate rotations (blue), shifts the period of India's fastest motion from Chron 29N to Chron 29R.

Downloaded from https://academic.oup.com/gji/article/200/1/227/749250 by guest on 18 February 2022

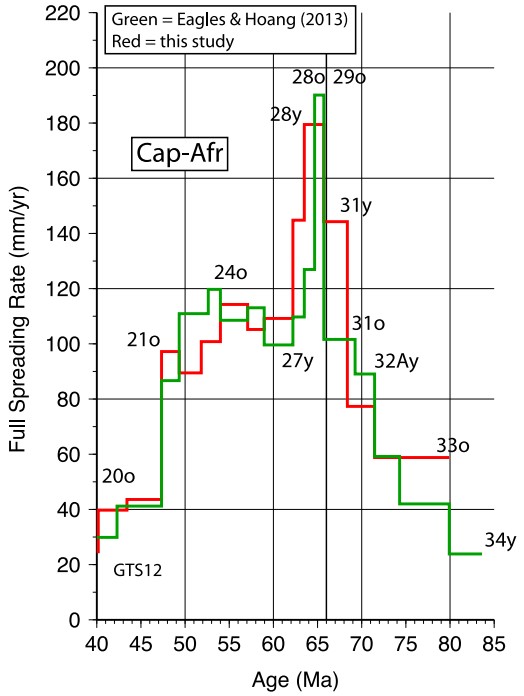


Figure 17. Comparison of Cap–Afr spreading rates for two sets of finite rotations. Spreading rates based on the finite rotations of Eagles & Hoang (2013) (green) display a shorter period of superfast spreading than rates based on the rotations presented here (red).

and then a very rapid rise between 31y and 30y from 80 to almost 180 mm yr^{-1}. This is followed by a short, 3 Ma, interval of superfast spreading, a sudden decline to 115 mm yr^{-1} between Chrons 28y and Chron 27y, and then a more gradual falloff from 115 to roughly 90 mm yr^{-1} at Chron 21o. The much more rapid drop after Chron 21o (47 Ma) is compatible with a collision event, although the sharp change in azimuth of Cap–Afr spreading, as noted by Cande *et al.* (2010), does not occur until after Chron 20o (43 Ma).

Based on their work in the Mascarene Basin, Eagles & Wibisono (2013) found that India's velocity relative to the mantle was characterized by a steady increase between Chrons 34y and 30o. They proposed that this increase was caused by a growing ridge push force in the Mascarene Basin. They attributed the pulse of superfast spreading to the effect of the ridge jump to the Laxmi Basin around Chron 30. Specifically, they proposed that the propagation of an anomalously shallow ridge crest into an already-thickened portion of the Indian Plate, led to an enhancement of the slope of the lithosphere–asthenosphere boundary at the edge of the plate, and an increase in the magnitude of the ridge push. They attribute only a small part of the pulse of superfast spreading to a plume head effect. Unfortunately, because of the difficulty in determining SEIR rotations for Chrons 34y and 33y, we were not able to independently derive as complete a CIR spreading history between Chrons 34 and 30 as the one presented by Eagles & Wibisono (2013). We do note that the pulse of superfast spreading around Chron 29 based on our CIR rotations was about twice as long in duration as their pulse. In addition, we do not see the velocity of India abruptly returning to its pre-68 Ma value at 64 Ma as was found by Eagles & Wibisono (2013). Instead we find that the velocity of India remained about 30 mm yr^{-1} above its pre-rapid acceleration value for about 10 myr (Fig. 17).

An examination of the four Indo-Atlantic spreading rate curves in the right-hand panel of Fig. 14 leads us to suggest that the first

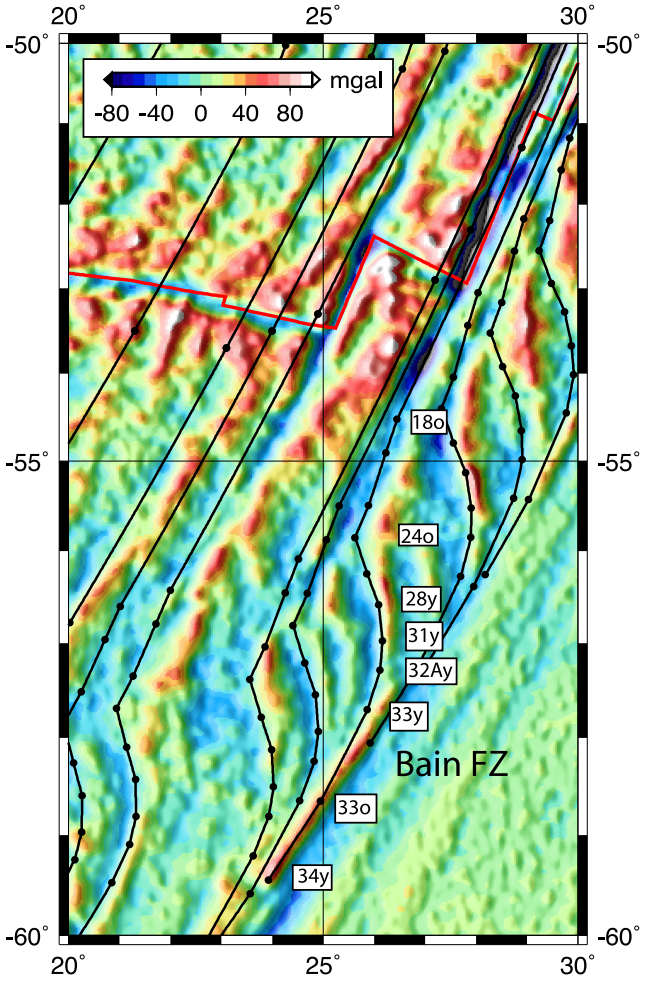


Figure 18. Demonstration that the change in the migration path of the SWIR stage poles at Chron 31y occurs shortly after the replacement of a few long transform faults on the Bain FZ with numerous short offset ridge segments. Black lines are synthetic flowlines based on the revised 2-plate finite rotations presented here superimposed on gravity anomalies constrained by satellite altimetry data.

indication of a plume head push effect on plate velocities may have been around Chron 32Ay (71 Ma). We note that there was an acceleration in India's velocity relative to Antarctica around Chron 32Ay which occurred at the same time that there was a sharp decrease in Africa's velocity relative to Antarctica and South America (Fig. 14). In the South Atlantic this slowdown was accompanied by a major jump in the ridge axis south of the Rio Grande Rise (Cande *et al.* 1988). Chron 32Ay was also the time of a notable change in the SWIR stage poles; they started to migrate to the southeast (Fig. 9). These changes occurred without any obvious tectonic events in the Mascarene Basin (the oldest fossil spreading centre in the north end is Chron 30y–about 66 Ma) although it may have occurred about the time of the initiation of spreading in the Gop Rift (Armitage *et al.* 2011).

A second notable change in Afr–Ant motion occurs around Chron 31y (68 Ma) when the path of the SWIR stage poles changes direction to the west–northwest (Fig. 9). This change occurs without any further slowing of Africa and is roughly coincidental with the development of multiple short ridge sections and transform faults that replaced the long transform faults on the Bain FZ. This is apparent from the satellite derived gravity imagery in Fig. 18 shown with

Downloaded from https://academic.oup.com/gji/article/200/1/227/749250 by guest on 18 February 2022

superimposed synthetic flow lines. The coincidence of these two events suggests that the change in the migration path of the SWIR stage poles may have been caused by a ridge push force generated by the multiple new ridge segments along the Bain FZ.

The sudden drop in Cap–Afr motion between Chrons 28y and 27y (63 to 62 Ma) is puzzling. As noted by Eagles & Wibisono (2013), this drop appears to occur more rapidly than is predicted from the simple plume head models of Van Hinsbergen *et al.* (2011). We note that there are no significant kinematic changes in motion on the SWIR or in the South Atlantic. Eagles & Wibisono (2013) note the synchroneity of this event with the jump of the locus of India–Seychelles rifting from the Laxmi Basin to the south side of the Laxmi Ridge and suggest that a sudden change in the ridge push force acting on India might have caused it, although they comment that it could also be attributed to other changes in plate boundary forces. It is an intriguing kinematic event.

Our analysis of the SWIR fracture zones shows that the change in direction of Afr–Ant motion following Chron 24o (54 Ma) was very abrupt, suggesting that it was driven by a major tectonic event. The cause of this regional change in motion is enigmatic. On the one hand, the age of 55 Ma is often associated with the initial collision of India with Eurasia (Garzanti *et al.* 1996; Garzanti 2008). However, as Figs 14 and 15 show, with the latest GPTS there is very little change in India's velocity (relative to Africa, Antarctica or the mantle) at this time; it precedes by at least 7 Ma the start of the rapid slowing of the Indian Plate at Chron 21o attributed to the initial collision of India with Eurasia (Molnar & Tapponier 1975; Patriat & Achache 1984; Copley *et al.* 2010). However, this is the time of significant tectonic changes in the Atlantic basins. For example, Chron 25/24 is the time of the onset of convergence between South America and North America plates along the Caribbean boundary (Müller *et al.* 1999). Chron 25/24 also corresponds to the rifting of Greenland and Norway which is often attributed to the onset of the Iceland plume head (White & McKenzie 1989). We speculate that plate kinematic changes associated with the onset of the Iceland plume head may be responsible for the sudden kinematic changes in the South Atlantic and SWIR that occurred at the same time.

8 SUMMARY AND CONCLUSIONS

We calculated a revised set of closely spaced finite rotations for the SWIR (Afr–Ant) and the SEIR (Cap–Ant) for anomalies 34 to 20 based on an updated interpretation of magnetic anomalies and fracture zones. This interpretation recognizes a much sharper bend in the SWIR fracture zones at Chron 24o than in Cande *et al.* (2010). In order to use a consistent set of data constraints for the entire time period, these rotations are all 2-plate solutions. Revised CIR (Cap–Afr) rotations were calculated by summing the SWIR and SEIR rotations.

The revised rotations better define the stage pole path followed by the SWIR; from Chrons 34y to 33y the stage poles were stationary, from Chrons 33y to 31y the stage poles migrated to the southeast, from Chrons 31y to 24o they migrated to the west–northwest, and after Chron 24o the poles moved rapidly back to the east. The revised CIR rotations suggest that the period of a separate Seychelles microplate on the Carlsberg ridge terminated before Chron 25y, about 7 Ma older than the age suggested by Cande *et al.* (2010) and consistent with the Chron 27 termination date suggested by Eagles & Hoang (2013).

An analysis of the relative velocities of India, Africa and Antarctica confirm the main observation of Cande & Stegman (2011) that the speedup of India was accompanied by a slowdown of Africa and vice versa. With the most recent changes to the geomagnetic polarity timescale (GTS12), the general shape of the velocity curve for India between 75 and 45 Ma looks roughly like the motion predicted by the simple plume head models of van Hinsbergen *et al.* (2011), although the magnitude of the actual speedup is larger by a factor of two. The fastest motion of India with respect to the mantle ($\sim$220 mm yr^{-1}) occurs within Chron 29R, the time of the maximum outpouring of Deccan flood basalts, and the period of superfast motion lasts about 3 Ma. However, the falloff in spreading rates following the period of superfast spreading, between Chrons 28y and 27y (63 to 62 Ma), is more rapid than the predictions of the simple plume head models presented by van Hinsbergen *et al.* (2011).

The earliest notable kinematic effects of the Reunion plume head may be around Chron 32Ay (71 Ma) when there was an acceleration of India's motion with respect to Antarctica and at the same time a rapid slowdown in Afr–Ant and Afr–Sam spreading rates. These anticorrelated spreading rate changes were accompanied by a change in the migration of the SWIR stage poles. In the South Atlantic the slowdown was accompanied by a major jump in the ridge axis south of the Rio Grande Rise.

The change in the migration path of the SWIR stage poles towards the west–northwest around Chron 31y starts shortly after the onset of extension along the Bain transform fault zone and the replacement of several long-offset transform faults with 8 or 10 short-offset ridge and transform fault sections, suggesting that it may reflect a ridge push force coming from the new ridge sections on the SWIR along the Bain FZ section of the ridge.

The abrupt change in the migration path of the Afr–Ant (SWIR) stage poles at Chron 25/24 is not associated with major changes in the velocities of either Africa or India and may reflect plate motion changes in the North Atlantic associated with the arrival of the Iceland plume head at the Earth's surface and the rifting of Greenland and Norway. The slowdown of India around Chron 21 is sharper with the GTS12 timescale than in previous timescales and, contrary to the suggestion of Cande & Stegman (2011), appears to be consistent with a collision event.

ACKNOWLEDGEMENTS

We thank Graeme Eagles and an anonymous reviewer for helpful comments. Support for this work was provided by NSF grant OCE1130047 to SCC.

REFERENCES

Armitage, J.J., Collier, J.S., Minshull, T.A. & Henstock, T.J., 2011. Thin oceanic crust and flood basalts: India-Seychelles breakup, *Geochem. Geophys. Geosyst.,* **12,** Q0AB07, doi:10.1029/2010GC003316.

Bergh, H.W., 1971. Sea floor spreading in the southwest Indian Ocean, *J. geophys. Res.,* **76,** 6276–6282.

Bernard, A. & Munschy, M., 2000. Le basin des Mascareignes et le basin de Laxmi (ocean Indien occidental) se sont-ils formes a l'axe d'un meme centre d'expansion? *Comptes Rendus del'Academie de Sciences Serie 2a,* **330,** 777–783.

Bernard, A., Munschy, M., Rotstein, Y. & Sauter, D., 2005. Reffined spreading history at the Southwest Indian Ridge for the last 96 Ma, with the aid of satellite gravity data, *Geophys. J. Int*., **162,** 765–778.

Bhattacharya, G.C., Chaubey, A.K., Murty, G.P.S., Srinivas, K., Sarma, K.V.L.N.S., Subrahmanyam, V. & Krishna, K.S., 1994. Evidence for seafloor spreading in the Laxmi Basin, northeastern Arabian Sea, *Earth planet. Sci. Lett.,* **125,** 211–220.

Downloaded from https://academic.oup.com/gji/article/200/1/227/749250 by guest on 18 February 2022

Cande, S.C. & Kent, D.V., 1995. Revised calibration of the geomagnetic polarity timescale for the Late Cretaceous and Cenozoic, *J. geophys. Res.,* **100,** 6093–6095.

Cande, S.C. & Stegman, D.R., 2011. Indian and African Plate motions driven by the push forvce of the Reunion plume head, *Nature,* **475,** 47–52.

Cande, S.C., LaBreque, J.L. & Haxby, W.F., 1988. Plate kinematics of the South Atlantic: Chron 34 to present, *J. geophys. Res.,* **93,** 13 479–13 492.

Cande, S.C., Patriat, P. & Dyment, J., 2010. Motion between the Indian, Antarctica and African plates in the early Cenozoic. *Geophys. J. Int.,* **183,** 127–149.

Chang, T., 1987. On the statistical properties of estimated rotations, *J. geophys. Res.,***92,** 6319–6329.

Chang, T., 1988. Estimating the relative rotation of two tectonic plates from boundary crossings, *J. Am. stat. Assoc*., **83,** 1178–1183.

Chenet, A.L., Quidelleur, X., Fluteau, F., Courtillot, V. & Bajpai, S., 2007. 40K–40Ar dating of the Main Deccan large igneous province: further evidence of KTB age and short duration. *Earth planet. Sci. Letts.,* **263,** 1–15.

Chu, D. & Gordon, R.G., 1999. Evidence for motion between Nubia and Somalia along the Southwest Indian Ridge, *Nature,* **398,** 64–67.

Collier, J.S., Sansom, V., Ishizuka, O., Taylor, R.N., Minshull, T.A. & Whitmarsh, R.B., 2008. Age of Seychelles–India break-up, *Earth planet. Sci. Lett.,* **272,** 264–277.

Copley, A., Avouac, J.-P. & Royer, J.-Y., 2010. India-Asia collision and the Cenozoic slowdown of the Indian Plate: implications for the forces driving plate motions, *J. geophys. Res.,* **115,** B03410, doi:10.1029/2009JB006634.

DeMets, C., Gordon, R.G. & Argus, D.F., 1988. Intraplate deformation and closure of the Australia-Antarctica-Africa Plate circuit, *J. geophys. Res.,* **93,** 11 877–11 897.

DeMets, C., Gordon, R.G. & Royer, J.-Y., 2005. Motion between the Indian, Capricorn, and Somalian plates since 20 Ma: implications for the timing and magnitude of distributed lithospheric deformation in the equatorial Indian Ocean, *Geophys. J. Int.,* **161,** 445–468.

Desa, M., Ramana, M.V. & Ramprasad, T., 2009. Evolution of the Late Cretaceous crust in the equatorial region of the Northern Indian Ocean and its implication in understanding the plate kinematics, *Geophys. J. Int.,* **177,** 1265–1278.

Duncan, R.A. & Richards, M.A., 1991. Hotspots, mantle plumes, flood basalts, and true polar wander, *Rev. Geophys.,* **29,** 31–50.

Dyment, J., 1991. Structure et evolution de la lithosphere oceanique dans l'ocean Indien: apport des anomalies magnetiques, *PhD thesis,* 374 pp., University of Louis Pasteur, Strasbourg, France.

Dyment, J., 1993. Evolution of the Indian Ocean Triple Junction between 65 and 49 Ma (anomalies 28 to 21), *J. geophys. Res.,***98,** 13 863–13 877.

Dyment, J., 1998. Evolution of the Carlsberg Ridge between 60 and 45 Ma: ridge propagation, spreading asymmetry, and the Deccan-Reunion hotspot, *J. geophys. Res.,* **103,** 24 067–24 084.

Eagles, G. & Hoang, H.H., 2013. Cretaceous to present kinematics of the Indian, African and Seychelles plates, *Geophys. J. Int.,* **196,** 1–14.

Eagles, G. & Wibisono, A.D., 2013. Ridge push, mantle plumes and the speed of the Indian plate, *Geophys. J. Int,* **194,** 670–677.

Garzanti, E., 2008. Comment on "When and where did India and Asia collide?" by Jonathan C. Aitchison, Jason R. Ali, and Aileen M. Davis, *J. geophys. Res.,***113,** B04411, doi:10.1029/2007JB005276.

Garzanti, E., Critelli, S. & Ingersoll, R.V., 1996. Paleogeographic and paleotectonic evolution of the Himalayan Range as reflected by detrital modes of Tertiary sandstones and modern sands (Indus transect, India and Pakistan), *Geol. Soc. Am. Bull.,* **108,** 631–642.

Gradstein, F.M. *et al.*, 2004. *A Geologic Time Scale 2004,* 589 pp, Cambridge Univ. Press.

Hellinger, S.J., 1981. The uncertainties of finite rotations in plate tectonics, *J. geophys. Res.,* **86,** 9312–9318.

Horner-Johnson, B.C., Gordon, R.G. & Argus, D.F., 2007. Plate kinematic evidence for the existence of a distinct plate between the Nubian and Somalian plates along the Southwest Indian Ridge, *J. geophys. Res.,* **112,** B05418, doi:10.1029/2006JB004519.

Kirkwood, B.H., Royer, J.-Y., Chang, T.C. & Gordon, R.G., 1999. Statistical tools for estimating and combining finite rotations and their uncertainties, *Geophys. J. Int.,* **137,** 408–428.

Lemaux, J., Gordon, R.G. & Royer, J.-Y., 2002. The location of the Nubia-Somalia boundary along the Southwest Indian Ridge, *Geology,* **30,** 339–342.

Liu, C, Curray, J.R. & McDonald, J.M., 1983. New constraints on the Tectonic evolution of the eastern Indian Ocean, *Earth. planet. Sci. Lett.,* **65,** 331–342.

Masson, D.G., 1984. Evolution of the Mascarene Basin, Western Indian Ocean and the significance of the Amirante arc, *Mar. Geophys. Res.,* **6,** 365–382.

McKenzie, D.P. & Sclater, J.G., 1971. The evolution of the Indian Ocean since the Late Cretaceous, *Geophys. J. R. astr. Soc.,* **25,** 437–528.

Minshull, T.A., Lane, C.I., Collier, J.S. & Whitmarsh, R.B., 2008. The relationship between rifting and magmatism in the Northeastern Arabian Sea, *Nat. Geosci.,***1,** 463–467.

Molnar, P. & Tapponnier, P., 1975. Cenozoic tectonics of Asia: effects of a continental collision, *Science,* **189,** 419–426.

Molnar, P., Pardo-Casas, F. & Stock, J., 1988. The Cenozoic and Late Cretaceous evolution of the Indian Ocean: uncertainties in the reconstructed positions of the Indian, African and Antarctic plates, *Basin Res.,* **1,** 23–40.

Müller, R.D., Royer, J.-Y. & Lawver, L.A., 1993. Revised plate motions relative to the hotspots from combined Atlantic and Indian Ocean hotspot tracks, *Geology,* **21,** 275–278.

Müller, R.D., Royer, J.-Y., Cande, S.C., Roest, W.R. & Maschenkov, S., 1999. New constraints on the Late Cretaceous/Tertiar y plate tectonic evolution of the Caribbean, in *Caribbean Basins,* Sedimentary Basins of the World, Vol. 4, pp. 33–59, ed. Mann, P., Elsevier Science.

Nankivell, A.P., 1997. Tectonic evolution of the Southern Ocean Between Antarctica, South America and Africa over the Last 84 Ma, *PhD thesis,* University of Oxford, p. 303.

Norton, I.O. & Sclater, J.G., 1979. A model for the evolution of the lndian Ocean and the breakup of Gondwanaland, *J. geophys. Res.,* **84,** 6803–6830.

Ogg, J.G., 2012. Geomagnetic polarity time scale, in *The Geologic Time Scale 2012,* pp. 85–112, eds Gradstein, F.M., Ogg, J.G., Schmitz, M.D. & Ogg, G., Elsevier Science.

Pande, K., 2002. Age and duration of the Deccan Traps, India: a review of radiometric and paleomagnetic constraints, *Proc. Indian Acad. Sci.* **111,** 115–123.

Patriat, P., 1987. *Reconstitution de l'évolution du système de dorsales de l'océan Indien par les méthodes de la cinématique des plaques,* 308 pp., Territoire des Terres Australes et Antarctiques Françaises, Mission de Recherche, Paris.

Patriat, P. & Achache, J., 1984. India-Eurasia collision chronology has implications for shortening and driving mechanism of plates, *Nature,* **311,** 615–621.

Patriat, P. & Segoufin, J., 1988. Reconstruction of the Central Indian Ocean, *Tectonophysics,* **155,** 211–234.

Patriat, P., Segoufin, J., Goslin, J. & Beuzart, P., 1985. Relative positions of Africa and Antarctica in the Upper Cretaceous: evidence for non-stationary behaviour of fracture zones, *Earth planet. Sci. Lett.,* **75,** 204–214.

Patriat, P., Sloan, H. & Sauter, D., 2008. From slow to ultraslow: a previously undetected event at the Southwest Indian Ridge at ca. 24 Ma, *Geology,* **36,** 207–210.

Plummer, P.S., 1996. The Amirante ridge/trough complex: response to rotational transform rift/drift between Seychelles and Madagascar, *Terra Nova,* **8,** 34–47.

Richards, M.A., Duncan, R.A. & Courtillot, V.E., 1989. Flood basalts and hotspot tracks: plume heads and tails, *Science,* **246,** 103–107.

Royer, J.Y. & Chang, T., 1991. Evidence for relative plate motions between the Indian and Australian plates during the last 20 m.y. from plate tectonic reconstructions: implications for the deformation of the Indo-Australian plate, *J. geophys. Res.,* **96,** 11 779–11 802.

Royer, J.-Y. & Gordon, R.G., 1997. The motion and boundary between the Capricorn and Australian plates, *Science,* **277,** 1268–1274.

Downloaded from https://academic.oup.com/gji/article/200/1/227/749250 by guest on 18 February 2022

Royer, J.Y. & Patriat, P., 2002. L'inde part a la derive, in *Himalaya-Tibet, Le Choc des Continents,* pp. 25–31, eds Allegre, C.J., Avouac, J.-P. & De Wever, P., Mus. Natl. de'Hist. Nat., Paris.

Royer, J.Y. & Sandwell, D.T., 1989. Evolution of the Eastern Indian Ocean since the Late Cretaceous: constraints from Geosat altimetry, *J. geophys. Res.,* **94,** 13 755–13 782.

Royer, J.Y., Chaubey, A.K., Dyment, J., Bhattacharya, G.C., Srinivas, K., Yatheesh, V. & Ramprasad, T., 2002. Paleogene plate tectonic evolution of the Arabian and Eastern Somali basins, in *The Tectonic and Climatic Evolution of the Arabian Sea Region,* pp. 7–23, eds Clift, P.D., Croon, D., Gaedicke, C. & Craig, J., Geological Society.

Royer, J.-Y., Gordon, R.G. & Horner-Johnson, B.C., 2006. Motion of Nubia relative to Antarctica since 11 Ma: implications for Nubia-Somalia, Pacific-North America, and India-Eurasia motion, *Geology,* **34,** 501–504.

Royer, J.-Y., Patriat, P., Bergh, H.W. & Scotese, C.R., 1988. Evolution of the Southwest Indian Ridge from the Late Cretaceous (Anomaly 34) to the Middle Eocene (Anomaly 20), *Tectonophysics,* **155,** 235–260.

Sandwell, D.T. & Smith, W.H.F., 1997. Marine gravity anomaly from Geosat and ERS-1 satellite altimetr y, *J. geophys. Res.,* **102,** 10 039–10 054.

Sclater, J.G., Munschy, M., Fisher, R.L., Weatherall, P.A., Cande, S.C., Patriat, P., Bergh, H. & Schlich, R., 1997. Geophysical synthesis of the Indian/Southern Oceans, Part 1: the Southwest Indian Ocean, Scripps Institution of Oceanography Reference Series 97-06, San Diego, La Jolla, Scripps Institute of Oceanography, University of California, p. 45.

Schlich, R., 1982. The Indian Ocean: aseismic ridges, spreading centers and basins, in *The Ocean Basins and Margins,* pp. 51–147, eds Nairn, A.E. & Stehli, F.G., Plenum.

Todal, A. & Edholm, O., 1998. Continental margin off Western India and Deccan large igneous province, *Mar. Geophys. Res.,* **20,** 273–291.

van Hinsbergen, D.J.J., Steinberger, B., Doubrovine, P.V. & Gassmäoller, R., 2011. Acceleration and deceleration of India-Asia convergence since the Cretaceous: roles of mantle plumes and continental collision, *J. geophys. Res.,* **116,** B06101, doi:10.1029/2010JB008051.

White, R.S. & McKenzie, D.P., 1989. Magmatism at rift zones: the generation of volcanic continental margins and flood basalts, *J. geophys. Res.,* **94,** 7685–7729.

Wiens, D.A. *et al.*, 1985. A diffuse plate boundary model for Indian Ocean tectonics, *Geophys. Res. Lett.,* **12,** 429–432.

Yatheesh, V., Bhattacharya, G.C. & Dyment, J., 2009. Early oceanic opening off Western India-Pakistan margin: the Gop Basin revisited, *Earth planet. Sci. Lett.,* **284,** 399–408.

Downloaded from https://academic.oup.com/gji/article/200/1/227/749250 by guest on 18 February 2022